Available online at www.sciencedirect.com

ScienceDirect

Geochimica et Cosmochimica Acta 164 (2015) 262–283

Geochimica et Cosmochimica Acta

www.elsevier.com/locate/gca

The cycling of iron, zinc and cadmium in the North East Pacific Ocean – Insights from stable isotopes

Tim M. Conway *, Seth G. John [1]

Department of Earth and Ocean Sciences, University of South Carolina, Columbia, SC 29208, USA

Received 14 November 2014; accepted in revised form 10 May 2015; available online 18 May 2015

Abstract

Dissolved stable isotope ratios of the transition metals provide useful information, both for understanding the cycling of these bioactive trace elements through the oceans, and tracing their marine sources and sinks. Here, we present seawater dissolved Fe, Zn and Cd concentration and stable isotope ratio (δ^{56}Fe, δ^{66}Zn, and δ^{114}Cd) profiles from two stations in the Pacific Ocean, the SAFe Station (30°N 140°W) in the subtropical North East Pacific from the GEOTRACES IC2 cruise, and the marginal San Pedro Basin (33.8°N 118.4°W) within the South California Bight. These data represent, to our knowledge, the first full-water column profiles for δ^{66}Zn and δ^{56}Fe from the open-ocean North Pacific, and the first observations of dissolved δ^{66}Zn and δ^{114}Cd in a low-oxygen marginal basin. At the SAFe station, δ^{56}Fe is isotopically lighter throughout the water column (−0.6 to +0.1‰, relative to IRRM-014) compared to the North Atlantic, suggesting significant differences in Fe sources or Fe cycling between these two ocean basins. A broad minimum in δ^{56}Fe associated with the North Pacific oxygen minimum zone (OMZ; <75 μmol kg^{-1} dissolved oxygen; ~550–2000 m depth) is consistent with reductive sediments along the California margin being an important source of dissolved Fe to the North Pacific. Other processes which may influence δ^{56}Fe at SAFe include biological cycling in the upper ocean, and input of Fe from hydrothermal vents and oxic sediments below the OMZ. Zn and Cd concentration profiles at both stations broadly match the distribution of the macronutrients silicate and phosphate, respectively. At SAFe, δ^{114}Cd increases towards the surface, reflecting the biological preference for assimilation of lighter Cd isotopes, while negative Cd* (−0.12) associated with low oxygen waters supports the recently proposed hypothesis of water-column CdS precipitation. In contrast to δ^{114}Cd, δ^{66}Zn at SAFe decreases towards the surface ocean, perhaps due to scavenging of isotopically heavy Zn, while at intermediate depths δ^{66}Zn provides further evidence of a mid-depth dissolved δ^{66}Zn maximum. We suggest this may be a global feature of Zn biogeochemistry related to either regeneration of heavy adsorbed Zn, or to ZnS formation and removal within the water column. Data from San Pedro shows that anoxic sediments can be a source of isotopically light Zn to the water column (δ^{66}Zn of ~−0.3‰ relative to JMC Lyon), though evidence of this signal is not observed being transported to SAFe. Within North Pacific Intermediate Water at SAFe (NPIW; ~500 m) elevated Cd* and Zn* and a focused minimum in δ^{56}Fe suggest possible transport of Fe, Zn, and Cd over thousands of km from subpolar waters, meaning that NPIW may have a strong influence on the subsurface distribution of trace metals throughout the North Pacific.

1. INTRODUCTION

Measurements of the stable isotope ratios of the transition metals are becoming useful oceanographic tools for the study of the marine biogeochemical cycling of these trace metals. There is great interest in understanding the cycling

* Corresponding author. Present address: Institute of Geochemistry and Petrology, Department of Earth Sciences, ETH Zürich, Clausiusstrasse 25, 8092 Zürich, Switzerland. Tel.: +41 44 632 4797.

E-mail address: conway.tm@gmail.com (T.M. Conway).

[1] Present address: Department of Earth Sciences, University of Southern California, Los Angeles, CA 90089, USA.

http://dx.doi.org/10.1016/j.gca.2015.05.023

0016-7037/

of trace metals such as Fe, Cu, Ni, Zn and Cd because of their roles as essential nutrients, or in some cases toxins, for marine phytoplankton. Their role in phytoplankton physiology means that trace metals ultimately influence primary productivity and the global carbon cycle (e.g. Morel and Price, 2003). Over the last 5–10 years, a combination of advances in chemical purification techniques, higher-resolution mass spectrometers and the onset of the International GEOTRACES program have facilitated the measurement of isotopic ratios of Fe (δ^{56}Fe), Cu (δ^{65}Cu), Ni (δ^{60}Ni), Zn (δ^{66}Zn) and Cd (δ^{114}Cd; ε^{114}Cd; ε^{112}Cd) dissolved in seawater. The first studies have shown that these ratios can be determined in seawater with sufficient precision and accuracy to observe variability at the permil level, even at the low concentrations of these metals in surface seawater (Bermin et al., 2006; Lacan et al., 2006, 2008; Ripperger and Rehkämper, 2007; Cameron and Vance, 2014). In the last few years, the first multiple-profile studies and oceanographic sections of δ^{56}Fe, δ^{66}Zn and δ^{114}Cd are beginning to appear as part of efforts such as the GEOTRACES program (e.g. Radic et al., 2011; Boyle et al., 2012; Abouchami et al., 2014; Conway and John, 2014a,b, 2015; Labatut et al., 2014; Zhao et al., 2014).

Combined with concentration data, stable isotope ratios of Fe, Zn and Cd provide valuable new information that can be used to investigate and understand the marine sources, cycling and sinks of these elements in a way that is not possible from concentration data alone. For example, studies have shown that different Fe sources have different δ^{56}Fe signatures, dependent on different chemical and biogeochemical processes, and that these δ^{56}Fe signatures persist great distances through the ocean. Reduced Fe released to the water column from low-oxygen pore-waters in benthic sediments is characterized by very light δ^{56}Fe values of −1.8 to −3.5‰ (e.g. Homoky et al., 2009; Severmann et al., 2010; John et al., 2012), while non-reductive Fe release from sediments and particles has been suggested to be 0 to +0.2‰ heavier than crustal values of +0.09‰ (proposed by Radic et al. (2011), and further observed by Homoky et al. (2013), Conway and John (2014a) and Labatut et al., (2014)). Recently, the δ^{56}Fe signature of Fe released from atmospheric dust was hypothesized to be much heavier (+0.68‰) than bulk natural crustal aerosol δ^{56}Fe (~+0.1‰; Beard et al., 2003; Waeles et al., 2007; Conway and John, 2014a), attributed to fractionation reactions upon dissolution in seawater, perhaps involving heavier Fe bound to organic ligands (Dideriksen et al., 2008; Morgan et al., 2010; John and Adkins, 2012; Conway and John, 2014a).

Hydrothermal Fe signatures are likely to depend on the vent chemistry and redox processes controlling distribution of Fe away from the vent (Severmann et al., 2004; Bennett et al., 2009). Very light hydrothermal dissolved δ^{56}Fe signatures have been recently documented within a hydrothermal plume at the Mid-Atlantic Ridge in the North Atlantic (−1.35‰; Conway and John, 2014a). Here, oxide precipitation is thought to dominate the system, resulting in dissolved δ^{56}Fe lighter than the vent fluids (Severmann et al., 2004; Conway and John, 2014a), but the net signature of release from other vents where sulfur chemistry is relatively more important could be heavy. Recent work has shown variable δ^{56}Fe signatures for distal hydrothermal signals in the Pacific Ocean, with the δ^{56}Fe of a hydrothermal Fe anomaly attributed to a distal EPR signal in the South Pacific ranging from −0.6 to +0.5‰ (Fitzsimmons et al., 2013, 2014). A recent study of a submarine volcano close to New Zealand showed a hydrothermal δ^{56}Fe signal that evolved from +0.1‰ to +1.7‰ as Fe was removed from the dissolved phase close to the vent (Ellwood et al., 2015), suggesting that the distal signal from this system could be remarkably heavy. However, despite these continuing uncertainties over hydrothermal source signals, we recently showed that it is possible to use δ^{56}Fe measurements to trace Fe sources over long distances and thus constrain the importance of different Fe sources across a North Atlantic section (Conway and John, 2014a). The short marine residence time of Fe, compared to other trace metals may also lead to significant inter-oceanic differences in δ^{56}Fe (Beard et al., 2003), which means that δ^{56}Fe can provide valuable information on the dominant Fe sources in each region.

Seawater-dissolved δ^{66}Zn measurements show promise for being able to understand the importance of processes such as scavenging, uptake and regeneration for the marine Zn cycle, as well as for understanding the global ocean mass balance of Zinc (Conway and John, 2014b; Little et al., 2014; Zhao et al., 2014), while dissolved δ^{114}Cd provide important insights about biological and physical cycling of Cd in the oceans (Ripperger et al., 2007). Phytoplankton are thought to preferentially acquire the light isotopes of Zn and Cd, while scavenging preferentially adsorbs heavy Zn isotopes to organic matter (Lacan et al., 2006; John et al., 2007a; Horner et al., 2013; John and Conway, 2014). In contrast to Zn, Cd is not thought to be scavenged to organic matter (John and Conway, 2014). Biological uptake of Zn and Cd therefore drive the resultant surface dissolved pool to heavier isotope ratios, while scavenging of Zn has the opposite effect on δ^{66}Zn (John and Conway, 2014). Isotopic ratios of both elements therefore provide information on the relative importance of different processes to the surface ocean cycling of these elements, and how this varies across the surface oceans. Fractionation of δ^{114}Cd due to biological uptake and incomplete regeneration in surface waters may lead to different preformed δ^{114}Cd signatures in different water masses, allowing investigation of the large scale cycling of Cd (Xue et al., 2013; Abouchami et al., 2014; Conway and John, 2015). Both elements have relatively homogenous signatures in the global deep oceans (δ^{114}Cd +0.2 to +0.3 and δ^{66}Zn +0.5‰), which are heavier than the isotopic signatures of their known sources (+0.1‰ for Cd; +0.1 to +0.3‰ for Zn), pointing to as-yet-unconstrained light sinks for both metals (Rehkämper et al., 2012; Janssen et al., 2014; Little et al., 2014; and references therein). One such sink may take the form of light biogenic Zn and/or Zn and Cd sulfides, precipitated directly within the water column (Conway and John, 2014b, 2015; Janssen et al., 2014; Janssen and Cullen, 2015).

Despite the community interest in these new tracers, the challenges of collection and analysis mean that there is still

little coverage to date in much of the world's oceans, especially in the Pacific Ocean. Historically, the North East Pacific was the focus of some of the first accurate studies of trace elements in the late 1970s – early 1980s, which demonstrated the now widely accepted oceanic relationships between Cd/phosphate and Zn/silicate, as well as Fe's role as a key limiting nutrient (Bruland et al., 1978a,b; Bruland, 1980; Coale et al., 1996). To date, the only North Pacific δ^{56}Fe data is from two marginal basins close to California and equatorial waters near Papua New Guinea (Radic et al., 2011; John et al., 2012; Labatut et al., 2014). δ^{66}Zn measurements are limited to two published Zn profiles above 1000 m (Bermin et al., 2006; John, 2007), and δ^{114}Cd is so far restricted to two profiles by Ripperger et al. (2007), although conference abstracts suggest a number of studies are in progress (e.g. Vance et al., 2012).

In this study, we present paired Fe, Zn and Cd isotope ratio and concentration profiles from two locations in the North East Pacific (Fig. 1), the open-ocean SAFe station (30°N 140°W), and the restricted San Pedro basin on the Californian Margin (33.8°N 118.4°W) that was previously studied for δ^{56}Fe by John et al. (2012). Using this data we: (1) discuss the sources and cycling of Fe and δ^{56}Fe in the open N. E. Pacific Ocean, (2) use Cd, Cd* and δ^{114}Cd to provide more insight into how biological uptake/regeneration, physical circulation and sulfide precipitation control dissolved Cd and δ^{114}Cd distributions, and (3) use δ^{66}Zn and Zn* data to investigate both how scavenging/regeneration of adsorbed Zn and/or sulfide precipitation may influence the distribution of dissolved Zn and how margin sediments can supply dissolved Zn to the ocean.

2. METHODS

2.1. Seawater sampling and oceanographic setting

A 12-depth seawater profile was collected from the SAFe site (30°N 140°W) in the North Pacific as part of a trace metal isotope cast (GT event 2066) on May 17th 2009, during the US GEOTRACES IC2 inter-comparison cruise. Seawater was collected by the onboard sampling

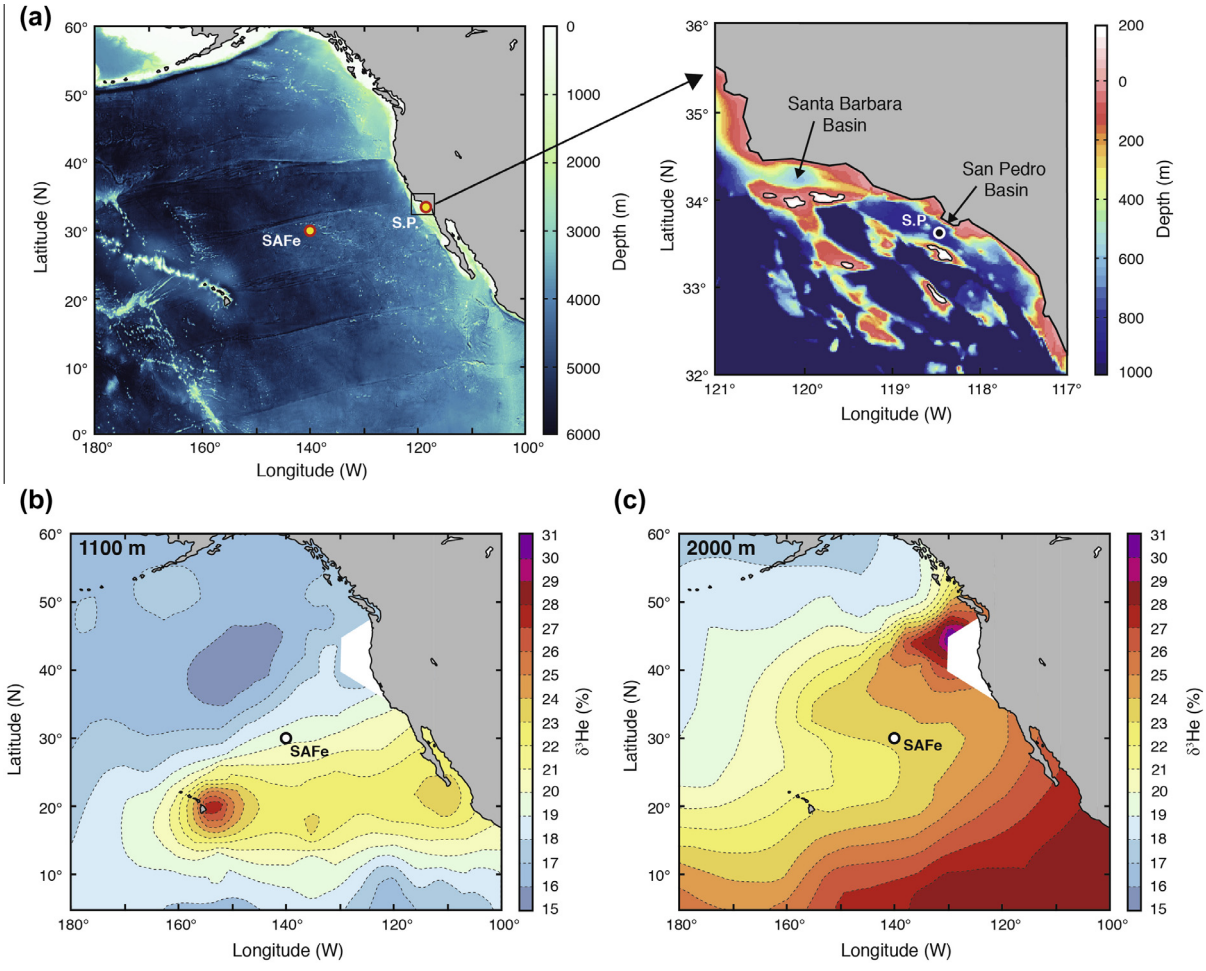

Fig. 1. Location of SAFe station (30°N 140°W) and San Pedro basin (33.8°N 118.4°W) sampling sites, overlaid on either (a) depth or δ^3He (%) at either (b) 1100 m or (c) 2000 m . δ^3He contours are based on Plate 4 of Lupton (1998), with 1100 m representing a Loihi hydrothermal source, and 2000 m representing the combined hydrothermal influence of Juan de Fuca and the East Pacific Rise. San Pedro is not shown overlaid on δ^3He because San Pedro basin depth is only 900 m. (For interpretation of colour in this figure, the reader is referred to the web version of this article.)

team using the GEOTRACES rosette and filtered with a 0.2 μm Osmonics capsule filter into acid-cleaned 1 L polyethylene bottles, according to published techniques (Cutter and Bruland, 2012). Seawater samples were collected from the San Pedro basin on the California Margin on board two cruises in September and October 2008 as part of the San Pedro Ocean Time Series (SPOT) program (John et al., 2012). San Pedro water samples were collected using 5 L Teflon-coated Niskin bottles mounted on a powder coated Rosette, or a Niskin bottle mounted on the ship's CTD rosette frame which was triggered during the downcast to minimize contamination (895 m only), and filtered through 0.4 μm Pall polyethersulfone filters (John et al., 2012). All filtered seawater samples were later acidified to pH ~2 by addition of 1 mL conc. QD-HCl and left for several years before processing and analysis of dissolved Fe, Zn and Cd concentrations and stable isotope ratios. The San Pedro samples used in this study were previously sub-sampled and analysed for dissolved Fe and δ^{56}Fe (John et al., 2012), and we do not present new Fe data for these here.

The SAFe station is located in the open North East Pacific Ocean (140°W, 30°N; Fig. 1), away from proximal sources of trace metals. The station is around 1900 km from the nearest continental shelf (California) or the nearest known hydrothermal sources (Juan de Fuca ridge and Loihi, Hawaii; Fig. 1). Atmospheric dust supply to this region is relatively low (0.2–0.5 g m^{-2} $year^{-1}$; Jickells et al., 2005). The distribution of trace metals in the water-column at this location are most strongly influenced by biological activity and *in situ* processes in surface waters (<500 m), transport of metals by large-scale ocean circulation, and the presence of a pronounced oxygen minimum zone at depths of ~550–2000 m (Figs. 2 and 3). The T-S water mass structure in this area of the North Pacific is well defined by Talley and coworkers and we follow their descriptions of the major water mass end-members (Talley, 2008; Talley et al., 2011). The subsurface water-mass structure (Figs. 2 and 3) consists of North Pacific Intermediate Water (NPIW; ~300–600 m; 26.7–26.9 σ_θ), Antarctic Intermediate Water (AAIW) mixed with NPIW (~600–1300 m; 26.9–27.6 σ_θ, salinity 34.14–34.45). Below this, Pacific Deep Water and modified Upper Circumpolar Deep Water (PDW & UCDW; <34.69, ~1300–3800 m, 1.1–1.2 °C,) and Lower Circumpolar (LCDW; >3800 m, >34.69 p.s.u.) are most important. NPIW is also characterized by a pronounced salinity minimum (<34.14 p.s.u.), reflecting its origins in subpolar waters in the Sea of Okhotsk, a northern marginal sea located between Siberia and Kamchatka, with transport from Asia via the Kuroshio currents (Talley, 1993; Talley et al., 2011).

The San Pedro basin, located within the South California Bight on the Californian Margin (~900 m deep; 33.8°N 118.4°W; Fig. 1), is a silled basin with a flat bottom, surrounded by broad shallow shelves (0–100 m) and characterized by low dissolved oxygen (John et al., 2012). The basin is silled below 740 m. Fully anoxic sediments with pore-water dissolved Fe concentrations up to 100 μmol L^{-1}, combined with dissolved oxygen concentrations as low as 2–5 μmol L^{-1} in overlying waters lead to dissolved Fe concentrations as high as 7.3 nmol L^{-1} within the water column (Severmann et al., 2010; John et al., 2012). John et al. (2012) interpreted high dissolved Fe concentrations and isotopically light δ^{56}Fe throughout the water-column as reflecting the input of isotopically light Fe(II) from benthic sediments. At shallow depths (50–100 m), lower-salinity, cold water indicates the subsurface presence of the California Current that moves south along the coast (Lynn and Simpson, 1987; Talley et al., 2011). Ekman transport and eddies provide variable upwelling of nutrients and trace metals from the benthic boundary layers to the California Current system along the Washington-Californian margin (e.g. King and Barbeau, 2011; Biller and Bruland, 2014). Localised eddy upwelling of Fe from shelf sediments can lead to dissolved Fe concentrations up to 8 nmol kg^{-1} in surface waters close to the Californian coast and islands (King and Barbeau, 2011). Deeper in the water column at San Pedro, at 150–200 m, the Californian Undercurrent moves northwards along the Californian margin from the Baja California (Talley et al., 2011). The San Pedro basin water column can therefore be thought of in terms of *in situ* vertical processes throughout the water column, as well as lateral advection in surface waters <200 m.

2.2. Sample processing and analysis

All seawater samples were processed at the University of South Carolina (USC) in flow benches under ULPA filtration, all water used was ultrapure (>18.2 MΩ) and all acids and reagents were Aristar Ultra™ obtained from VWR International. Dissolved Fe, Zn and Cd concentrations and stable isotope ratios were determined by Thermo Neptune MC-ICPMS with Jet interface in the Center for Elemental Mass Spectrometry at USC using isotope dilution and the double-spike technique. Samples were analyzed following extraction of metals from seawater with Nobias PA1 resin and purification with AGMP-1 anion exchange chromatography. The methodology used in this study, as well as the excellent precision and accuracy for isotopes ratios obtained by this technique, have already been described at some length (Conway et al., 2013; Conway and John, 2014a,b, 2015), and so will not be discussed in detail here. We also previously demonstrated that dissolved concentration measurements made using this method agree well with the most recent (May 2013) consensus values for SAFe seawater standards (Conway et al., 2013).

We express all stable isotope ratios in delta notation, relative to international isotope standards:

$$\delta^{56}\mathrm{Fe}\ (‰) = \left[\frac{\left(\frac{^{56}\mathrm{Fe}}{^{54}\mathrm{Fe}}\right)_{\mathrm{sample}}}{\left(\frac{^{56}\mathrm{Fe}}{^{54}\mathrm{Fe}}\right)_{\mathrm{IRMM\text{-}014}}} - 1\right] * 1000 \quad (1)$$

$$\delta^{66}\mathrm{Zn}\ (‰) = \left[\frac{\left(\frac{^{66}\mathrm{Zn}}{^{64}\mathrm{Zn}}\right)_{\mathrm{sample}}}{\left(\frac{^{66}\mathrm{Zn}}{^{64}\mathrm{Zn}}\right)_{\mathrm{JMC\ Lyon}}} - 1\right] * 1000 \quad (2)$$

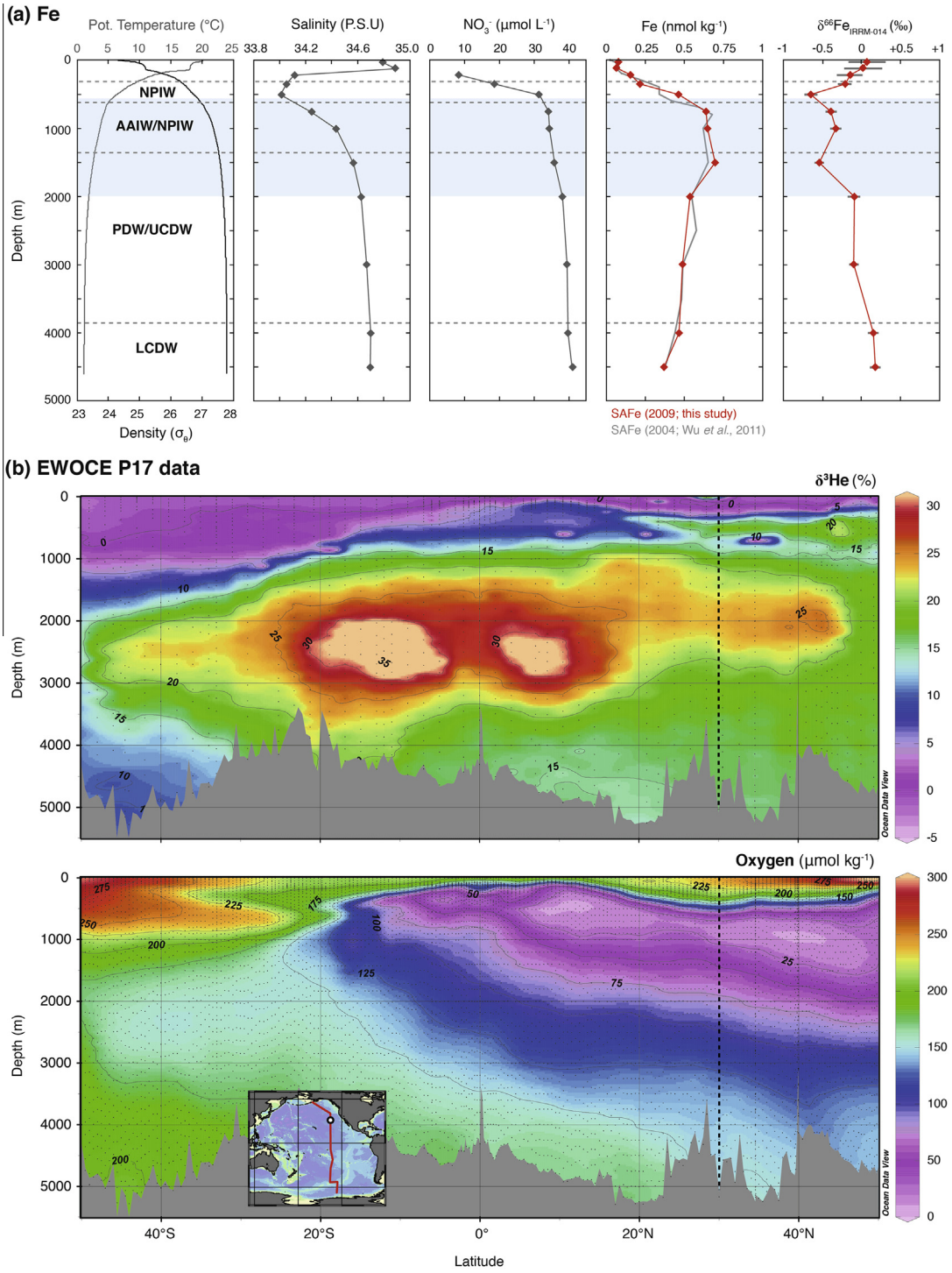

Fig. 2. Dissolved Fe concentration and stable isotope ratio (δ^{56}Fe) profiles from the SAFe Station in the North East Pacific (30°N 140°W; May 2009), with supporting dissolved data. The grey dissolved Fe data was measured in 0.4 µm filtered samples collected from the same location in October 2004 (Wu et al., 2011; here converted from nmol L^{-1} to nmol kg^{-1} using a seawater density of 1.025). The shaded blue bar represents dissolved oxygen concentrations <75 µmol L^{-1} (see Fig. 3a). Horizontal dashed lines represent delineation of water masses (see text; Talley, 2008; Talley et al., 2011): North Pacific Intermediate Water (NPIW), Antarctic Intermediate Water (AAIW), Upper Circumpolar Deep Water (UCDW), Pacific Deep Water (PDW), Lower Circumpolar Deep Water (LCDW). Errors on δ^{56}Fe are 2σ internal error as calculated in the text. (b) Dissolved δ^{3}He and oxygen concentrations from EWOCE P17 section (July 1991–June 1993). The vertical thick dashed line represents the location of the SAFe station on this section. (For interpretation of the references to colour in this figure legend, the reader is referred to the web version of this article.)

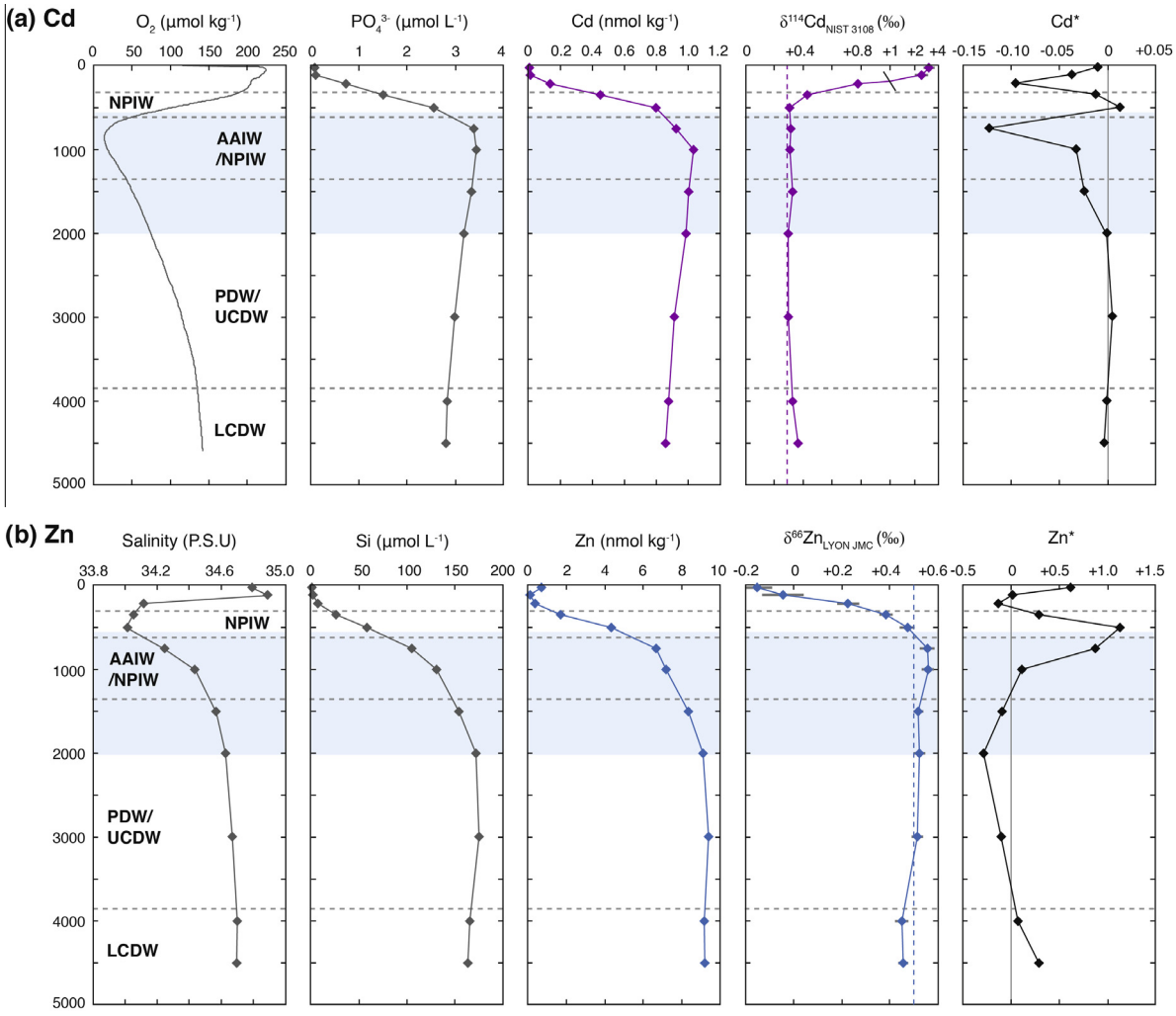

Fig. 3. Dissolved (a) Cd and (b) Zn concentrations and stable isotope ratio (δ^{114}Cd and δ^{66}Zn) profiles from the SAFe station in the North East Pacific (30°N 140°W), with supporting dissolved data. Note reduced scale for δ^{114}Cd above +1‰. The shaded blue bar represents dissolved oxygen concentrations <75 μmol L^{-1}. Vertical blue and purple dashed lines represent representative δ^{66}Zn (+0.5‰) and δ^{114}Cd (+0.3‰) of the deep ocean (see text). Horizontal dashed lines represent delineation of water masses as for Fig. 2. Zn^* and Cd^* are calculated as in the text, with 0 represented by a vertical grey line. All errors on isotope ratios are 2σ internal error as calculated in the text. (For interpretation of the references to colour in this figure legend, the reader is referred to the web version of this article.)

$$\delta^{114}\mathrm{Cd}\ (‰) = \left[\frac{\left(\frac{^{114}\mathrm{Cd}}{^{110}\mathrm{Cd}}\right)_{\mathrm{sample}}}{\left(\frac{^{114}\mathrm{Cd}}{^{110}\mathrm{Cd}}\right)_{\mathrm{NIST\ SRM\ 3108}}} - 1\right] * 1000 \quad (3)$$

For δ^{66}Zn, all samples were measured relative to NIST SRM 682 Zn and then are expressed relative to JMC Lyon by adjustment by −2.46% based on repeated analysis of the separation between the two standards (Conway et al., 2013; Conway and John, 2014b). Metal from each 1 L sample was measured twice by MC-ICPMS for each element, and the mean values are shown in figures. Following a detailed discussion of uncertainties affecting double spike ICP-MS measurements obtained with this procedure, and the repeated observation that total uncertainty is dominated by internal error (John, 2012; Conway et al., 2013), we express 2σ uncertainty on all stable isotope measurements as the combined standard internal error of samples and bracketing isotope standards. Equally, for dissolved elemental concentrations, we follow Conway et al. (2013) and apply 2% uncertainty to account for weighing, pipetting and calibration uncertainties.

For isotope mass balance calculations in Sections 3.1.2 and 3.4, we use a simple two-component isotope mass balance equation, that allows the calculation of the contribution of two different sources to the dissolved reservoir, each with a distinctive isotopic signature:

$$\delta^{x}\mathrm{Me}\ (‰) = (f_{source\ 1} \times \delta^{x}\mathrm{Me}_{source\ 1}) + (f_{source\ 2} \times \delta^{x}\mathrm{Me}_{source\ 2}) \quad (4)$$

Where δ^{x}Me denotes either δ^{56}Fe or δ^{66}Zn and f denotes the fraction of the dissolved Fe or Zn contributed from each of the two sources assuming $f_{source\ 1}$ and $f_{source\ 2}$ add up to 1.

2.3. Other oceanographic parameters

Salinity, dissolved phosphate (PO_4^{3-}) and dissolved silicate (Si) concentrations were previously measured for each bottle at the SAFe station on board the IC2 cruise using standard techniques, while density, potential temperature and dissolved oxygen are taken from shipboard CTD data. Dissolved phosphate and silicate were measured on San Pedro samples using standard techniques in the Benitez-Nelson lab at U.S.C. (Koroleff, 1983), and have an associated uncertainty of ~1% (~3% below 1 μmol kg^{-1}). Other San Pedro parameters are taken from John et al. (2012).

2.4. Dissolved Cd* and Zn*

Cd* and Zn* are parameters that can be used to show variability in the relationship between Cd and PO_4^{3-} or Zn and Si in the water column (Baars et al., 2014; Janssen et al., 2014; Wyatt et al., 2014). These are useful when investigating in-situ processes that might affect the trace metals but not the macronutrients. In this study we calculate Cd* and Zn* following the equations used in Janssen et al. (2014) and Conway and John (2014b, 2015):

$$Cd^* = [\mathrm{Cd}]_{\mathrm{measured}} - \left(\mathrm{Cd}/\mathrm{PO}_4^{3-}{}_{\mathrm{deep}} * [\mathrm{PO}_4^{3-}]_{\mathrm{measured}}\right) \quad (5)$$

$$\mathrm{Zn}^* = [\mathrm{Zn}]_{\mathrm{measured}} - \left(\mathrm{Zn}/\mathrm{Si}_{\mathrm{deep}} * [\mathrm{Si}]_{\mathrm{measured}}\right) \quad (6)$$

where [Cd] and [Zn] are expressed in nmol kg^{-1}, [PO_4^{3-}] or [Si] in μmol kg^{-1} (converted from measured μmol L^{-1} using a density of 1.025). Cd* and Zn* are relative parameters designed to highlight variability and so are expressed relative to reference ratios. In this study we set $(Cd/PO_4^{3-})_{deep}$ (0.317) and Zn/Si_{deep} (0.056) to the mean of the measured ratios ⩾2000 m at the SAFe station (see Supplementary Data), to represent deep Pacific waters below the influence of low-oxygen (<75 μmol L^{-1}) waters. We express uncertainty on Cd* and Zn* values (Supplementary Information) using standard error propagation of the uncertainty of Cd, Zn, PO_4^{3-} and Si concentration measurements (see Sections 2.2 and 2.3).

3. RESULTS AND DISCUSSION

Water-column concentration and stable isotope ratio profiles for dissolved Fe, Zn and Cd at SAFe are shown in Figs 2, 3 and 4. Water column concentration and isotope profiles for dissolved Fe, Zn and Cd at San Pedro are shown in Fig. 5, with Fe reproduced from John et al. (2012). We begin by discussing data from SAFe and the processes that control the distribution of each element there, and then go on to discuss the same for Cd and Zn at San Pedro.

3.1. Fe and δ^{56}Fe at SAFe

3.1.1. Patterns in dissolved Fe and δ^{56}Fe

The dissolved Fe concentration and δ^{56}Fe profiles measured from SAFe are shown in Fig. 2a. At SAFe, the water column was characterized by low Fe concentrations in the surface ocean (<0.1 nmol kg^{-1}; <100 m), a Fe maximum at intermediate depths (0.7 nmol kg^{-1}; 1000–1500 m) and lower Fe concentrations within deep Pacific waters (~0.4–0.5 nmol kg^{-1} > 2000 m). δ^{56}Fe values throughout the water column at SAFe ranged from −0.6 to +0.1‰, with isotopically lighter δ^{56}Fe (−0.33 ± 0.06 to −0.55 ± 0.06‰) corresponding to the depths of the oxygen minimum zone (<75 μmol kg^{-1}; ~550–2000 m; Figs. 2 and 3). The lightest δ^{56}Fe values were observed just above the OMZ, within NPIW at 500 m (−0.64 ± 0.08‰), and at the dissolved Fe concentration maximum at 1500 m (0.7 nmol kg^{-1}; −0.55 ± 0.06‰), while the heaviest δ^{56}Fe were observed close to the surface (+0.02 ± 0.24‰ and +0.07 ± 0.25‰) where Fe concentrations are low, and in deep waters below 3800 m (+0.15 ± 0.07‰ and +0.18 ± 0.07‰; Fig. 2a).

The dissolved Fe concentration profile from SAFe in this study (collected May 2009) is very similar to that reported by Wu et al. (2011) for a SAFe profile collected in 2004 (grey line, Fig. 2a), suggestive of a relatively stable Fe cycle over this timescale. Measurement of isotopically light δ^{56}Fe at 1000 m in this study (−0.33 ± 0.06‰) is consistent with our previous measurements in SAFe D1 and D2 reference standards, collected from 1000 m at SAFe in 2004 (−0.24 ± 0.05‰ to −0.39 ± 0.12‰; Conway et al., 2013). Our measured δ^{56}Fe values in D1 and D2 standards (Table 3 of Conway et al., 2013) were within error of each other, despite D1 suffering from precipitation of up to ~30% during sub-sampling from the un-acidified SAFe 1000 L tank, presumably due to wall adsorption/precipitation (Johnson et al., 2007). Thus, precipitation of Fe within the tank proceeded with apparently negligible fractionation of Fe isotopes. This increases our confidence in the fidelity of δ^{56}Fe measurements for similar samples obtained from deep low-oxygen waters that could potentially be compromised by similar processes, albeit on a lesser scale.

The vertical structure of dissolved Fe and δ^{56}Fe at SAFe, with higher concentrations of lighter Fe at 500–2000 m, largely associated with the OMZ, and lower concentrations of heavier δ^{56}Fe both above and below this horizon, should be considered in the context of possible vertical and horizontal processes. In the surface ocean, vertical *in situ* processes that have the potential to influence Fe and δ^{56}Fe include (1) mineral dust deposition and dissolution, (2) biological uptake in surface waters with regeneration at depth, and (3) vertical upward mixing and scavenging/precipitation of Fe from OMZ conditions to higher oxygen waters. In the intermediate and deep ocean, lateral transport of Fe, either within water masses or carried throughout low-oxygen waters within the North Pacific OMZ (~550–2000 m), may be a strong influence on dissolved δ^{56}Fe. Below, we discuss the possible effects of these various processes on the distribution of dissolved δ^{56}Fe and Fe at SAFe.

3.1.2. Vertical and in situ processes influencing δ^{56}Fe in surface waters

Over the top ~350 m, where dissolved Fe is ⩽0.2 nmol kg^{-1}, δ^{56}Fe values are slightly isotopically light or crustal (−0.2 to +0.1‰), and heavier than at intermediate depths (−0.4 to −0.6‰). There are several possible processes

which could cause this pattern. Perhaps the simplest idea would be a contribution of isotopically heavy Fe from atmospheric dust mixing with isotopically light Fe from below, accompanied by little-to-no fractionation during biological uptake/regeneration. If biological uptake/regeneration takes place with negligible δ^{56}Fe fractionation, uptake/regeneration will be indistinguishable from vertical mixing. If the net δ^{56}Fe signature of mineral dust in the North Pacific is similar to that suggested for the North Atlantic (+0.68‰; John and Conway, 2014), a rough mass balance calculation using Eq. (4) would suggest that δ^{56}Fe data over the surface 200 m could be explained by a 40–50% contribution from mineral dust and 50–60% contribution from upwelling of light Fe (−0.64‰ at 500 m).

Alternatively, it is possible that biological uptake of light Fe drives the surface ocean to heavier values, and then potentially regenerates deeper in the water column (Radic et al., 2011; Ellwood et al., 2015). However, there are few direct culture or open-ocean studies so far, and evidence for such a strong fractionation of δ^{56}Fe by biological uptake is mixed, suggesting a complex interplay of biological processes may interact to influence δ^{56}Fe. Illustrating this, a recent study of bloom development in the sub-tropical Pacific suggested that smaller phytoplankton may take up light Fe, driving the dissolved pool to heavier values, while diatom uptake of Fe showed no δ^{56}Fe fractionation (Ellwood et al., 2015). The same study also suggested that light δ^{56}Fe in surface waters (0–125 m) prior to bloom development could be caused by bacterial or photochemical reduction of Fe (Ellwood et al., 2015). Our recent study from the North Atlantic showed no clear evidence for the biological uptake of light Fe, but instead demonstrated a decrease in δ^{56}Fe near the fluorescence maximum which is consistent with a preferential biological removal of heavy Fe isotopes or release of light Fe by biological processes (Conway and John, 2014a). Consequently, while biological activity may affect δ^{56}Fe in surface waters, both the magnitude and direction of these processes on δ^{56}Fe at SAFe remain unclear. Regardless, the effects of biological processes on δ^{56}Fe are likely to be limited to depths above 500 m, where most other nutrient elements (e.g. N, P, Cd) are regenerated.

Another factor to consider is that oxidation/precipitation reactions and particle adsorption/desorption might fractionate Fe isotopes. At SAFe, oxidation and precipitation of Fe as waters are vertically mixed from OMZ depths (~550–2000 m) to higher oxygen conditions might lead to redox-associated fractionation (Johnson et al., 2002; Skulan et al., 2002; John et al., 2012). However, there are few field studies available to constrain the effect of these processes on δ^{56}Fe under open ocean conditions. Changes in δ^{56}Fe associated with oxidation/precipitation have been observed in the Baltic Sea, where δ^{56}Fe changed from −0.4‰ to +0.3‰ across the anoxic–oxic boundary (Staubwasser et al., 2013). However, this was associated with an order of magnitude change in Fe concentrations (450 to 30 nmol kg^{-1}; Staubwasser et al., 2013), suggesting that effects might be much more muted in open-ocean settings where Fe is present at lower concentrations and changes in Fe across OMZ boundaries are much smaller (this study; Conway and John, 2014a). Similarly, precipitation of Fe(III) within the water column of the San Pedro basin was modeled with a $\Delta\delta^{56}Fe_{particle\text{-}dissolved}$ of −0.8‰ (John et al., 2012); however, at San Pedro, high Fe concentrations and related rapid precipitation of dissolved Fe(III) might lead to a different Fe isotope effect than in open-ocean settings. Indeed, at SAFe the pattern in δ^{56}Fe and Fe provides little evidence for dramatic precipitation at the top of the OMZ (Fig. 2a). Dissolved Fe only drops from 0.64 to 0.47 nmol kg^{-1} between 750 and 500 m depth, despite oxygen rising over this interval from 19 to 100 μmol kg^{-1}. Additionally, δ^{56}Fe become lighter through this range (−0.4 to −0.6‰), rather than heavier. Taken together, this pattern suggests it is unlikely that the heavier δ^{56}Fe at depths shallower than 500 m are the result of *in situ* precipitation. Relatively small changes to dissolved Fe and δ^{56}Fe associated with increasing oxygen at SAFe might be because light dissolved Fe within the OMZ is already largely present as Fe(III), limiting fractionation between dissolved Fe(II)–Fe(III), which can cause large changes in δ^{56}Fe (Johnson et al., 2002). Although we have no speciation data, this idea would be consistent with other field studies which suggest that isotopically light Fe above sediments is present as Fe(III) but retains the light δ^{56}Fe signature of reduced sediment Fe(II) (John et al., 2012; Conway and John, 2014a; Sedwick et al., 2015).

While the *in situ* effects of precipitation and particle adsorption/desorption on δ^{56}Fe remain unclear and a full understanding will require future detailed experiments, we note that apparent negligible fractionation due to adsorption/precipitation in the SAFe tank also lends support to the idea that precipitation of Fe(III) within the open-ocean water column may not greatly change δ^{56}Fe source signatures. This would be consistent with the broad scale patterns of δ^{56}Fe in the North Atlantic and evidence from locations such as San Pedro (John et al., 2012; Conway and John, 2014a), which suggest that dissolved δ^{56}Fe retains source signatures during mixing and transport, making it possible to use δ^{56}Fe as a tracer of Fe sources through the ocean.

3.1.3. Tracing Fe sources at SAFe with δ^{56}Fe

Over the last two decades, a key goal of ocean biogeochemical modeling studies has been to understand how Fe is supplied to the surface ocean where it can be assimilated as a nutrient by phytoplankton. Initially, models focused on the dominance of Fe supplied by aeolian dust to the oceans, largely not considering other sources of Fe (e.g. Archer and Johnson, 2000; Moore et al., 2001; Aumont et al., 2003; Parekh et al., 2004). As field data and modeling studies have advanced, shelf sediments have been subsequently considered as an important source of Fe (e.g. Elrod et al., 2004; Jeandel et al., 2011), with newer models accordingly incorporating a sediment component (e.g. Moore et al., 2004; Moore and Braucher, 2008; Tagliabue et al., 2009). Most recently, the importance of hydrothermal sources of Fe to the ocean has been a focus for research, with long distance transport documented, perhaps due to stabilization with organic molecules (Boyle et al., 2005; Boyle and Jenkins, 2008; Toner et al., 2009; Tagliabue

et al., 2010; Wu et al., 2011; Saito et al., 2013; Fitzsimmons et al., 2014). Thus, hydrothermal Fe may be a much more important source than previously considered, especially in the Southern Ocean and South Pacific (Tagliabue et al., 2009), with a recent study suggesting that hydrothermal Fe from the East Pacific Rise travels as far west as New Zealand (~6000 km; Fitzsimmons et al., 2014). The importance of hydrothermal supply is accordingly considered by the latest ocean biogeochemical models (Tagliabue et al., 2010, 2014), and the aims of recent δ^{56}Fe and modeling studies have been to constrain the relative contributions from multiple Fe sources to the oceans (Conway and John, 2014a; Tagliabue et al., 2014).

In the Pacific, where dust deposition is relatively low (Jickells et al., 2005), non-dust sources such as sediments or hydrothermal venting may be more dominant than traditionally considered. δ^{56}Fe provides the opportunity to inform such hypotheses about the sources of Fe to the ocean, though they rely on an assumption that source δ^{56}Fe is not greatly modified during subsequent transport and reaction. While both the specific conditions under which source δ^{56}Fe may be modified during transit and different source end-members are not yet fully constrained, δ^{56}Fe does seem to be a tracer for Fe sources over great distances under typical open ocean conditions (Conway and John, 2014a). Thus, δ^{56}Fe data from SAFe provides us with the means to begin to investigate the sources of Fe to this region.

Although δ^{56}Fe data from the open North Pacific is very limited, with only three published seawater studies from marginal environments (Radic et al., 2011; John et al., 2012; Labatut et al., 2014), it can offer some insights into the sources of dissolved Fe. Indeed, the most striking observation about the δ^{56}Fe data at SAFe is the absence of isotopically heavy Fe throughout the entire water column, in contrast to our recently published δ^{56}Fe section for the North Atlantic Ocean where δ^{56}Fe away from hydrothermal and sedimentary sources was typically +0.4‰ to +0.8‰ (Conway and John, 2014a). There, we attributed the isotopically heavy Fe values to Fe released from atmospheric dust, reflecting fractionation during dissolution, perhaps associated with organic ligands (Conway and John, 2014a). The fact that δ^{56}Fe values >+0.1‰ are not observed at SAFe, where dust deposition is much lower than in the subtropical North Atlantic (<0.5 vs. 0.5–10 g m^{-2} year^{-2}; Jickells et al., 2005), combined with the observation that the heaviest δ^{56}Fe values are observed nearest the surface, is consistent with this hypothesis. Similarly, a recent observation of δ^{56}Fe of +0.3 to +0.4‰ in Equatorial Pacific bulk aerosols (Labatut et al., 2014) provides evidence for an isotopically heavy aerosol source. Thus, data from SAFe are supportive of our previous attribution of heavy Atlantic δ^{56}Fe to dust, and are also consistent with an evolving picture that an atmospheric supply of Fe is much less important in the North Pacific than in the North Atlantic.

At SAFe, instead of a dominant atmospheric source, we suggest that the light δ^{56}Fe and high Fe concentrations at depths of ~500–2000 m are indicative of lateral supply of isotopically light Fe. Two possible sources for this isotopically light Fe are reduced margin sediment pore-waters and hydrothermal venting. The heavier Fe in surface waters would then be attributed to either biological removal of light Fe or input from a heavier Fe source such as dissolution of atmospheric dust. Reductive sedimentary Fe in sediment pore-waters on the nearby North American continental margin is isotopically light (as light as −3.4‰; Homoky et al., 2009; Severmann et al., 2010; John et al., 2012), and while the net δ^{56}Fe signatures of hydrothermal source signals are currently poorly constrained, any Pacific hydrothermal source responsible for light δ^{56}Fe would by definition also be light. δ^{56}Fe measurements alone thus cannot distinguish between isotopically light sedimentary and hydrothermal Fe, and so we must also consider the broad scale pattern of other parameters such as Fe concentration and hydrothermal tracers such as δ^{3}He from other studies.

Recently, hydrothermal Fe and δ^{56}Fe signatures have been shown to be traceable over 1000–2000 km in the Atlantic (Saito et al., 2013; Conway and John, 2014a). If Fe is stabilized in the form of nano-particulate sulfides from sulfide-rich vent fluids which are common in Pacific hydrothermal systems, it might travel even greater distances in the Pacific (Yucel et al., 2011). This idea is supported by observational studies which found hydrothermally-derived Fe up to 6000 km away from vent sites (Wu et al., 2011; Fitzsimmons et al., 2014). It is therefore feasible that hydrothermal Fe could be transported from either Loihi or Juan de Fuca, which are both ~2000 km away, to SAFe. However, hydrothermal activity and the lateral transport of dissolved Fe can be traced using elevated δ^{3}He (e.g. Wu et al., 2011; Saito et al., 2013). Although widespread hydrothermal δ^{3}He anomalies are observed within the intermediate depth North Pacific (1000–2000 m; Figs. 1, 2b.), at SAFe both the dissolved Fe maximum at 1500 m and isotopically light Fe at 500–1500 m correspond poorly to the δ^{3}He maximum (1800–2200; Fig. 2b). This suggests that a hydrothermal source is unlikely to be responsible for the light Fe observed at SAFe from 500–2000 m.

The second possibility is lateral transport of Fe from a light sedimentary margin source, through the low-oxygen horizon at ~550–2000 m. Release of Fe(II) under low-oxygen conditions results in very isotopically light δ^{56}Fe (~−3‰) both in pore-waters on the Californian Margin and also within the water column of the Californian low-oxygen San Pedro and Santa Barbara basins (Homoky et al., 2009; Severmann et al., 2010; John et al., 2012). The data of John et al. (2012) showed that the light δ^{56}Fe signature from sediments was widespread within the water column of these restricted basins, allowing for this light δ^{56}Fe signature to be upwelled into the Californian Current and/or transported into the open ocean Pacific (e.g. Biller and Bruland, 2013). Consistent with the idea of reduced margin Fe being transported out into the open ocean Pacific, previous work also showed a large dissolved Fe plume (0.8–1.2 nmol kg^{-1}) present within the North Pacific OMZ, extending from the Californian margin all the way to the SAFe station (Johnson et al., 1997). That pattern, with Fe concentrations decreasing away from the margin, but with concentrations of

~0.8 nmol kg^{-1} at ~1000–1600 m reaching SAFe (Johnson et al., 1997) is consistent with the attribution of isotopically light Fe at SAFe to a sedimentary source. Taken together, the pattern of different datasets suggests that Californian Margin sediments are a likely source for the light Fe within the OMZ at SAFe.

3.1.4. Variability in δ^{56}Fe between 500 and 2000 m depth

Set against the general idea of a reductive sedimentary source of Fe to OMZ waters at ~550–2000 m, we do observe variability in δ^{56}Fe between 500–2000 m. The minimum in δ^{56}Fe at 1500 m (-0.55 ± 0.06‰) is consistent with the idea of a plume of sedimentary Fe extending from the Californian Margin with maximum extent at depths of ~1000–1600 m (Johnson et al., 1997). The presence of slightly heavier δ^{56}Fe values at depths of 750–1000 m (-0.3 to -0.4‰), where Fe concentrations are slightly lower, is also consistent with the idea of a lessening influence of sediment Fe at shallower depths within the OMZ as oxygen concentration rises. At 500 m, where oxygen has risen to 100 μmol kg^{-1}, we might expect an even smaller contribution from the Californian Margin and even heavier δ^{56}Fe. Instead, we observe the lightest δ^{56}Fe anywhere in the water column at SAFe at 500 m (-0.64 ± 0.08‰). This could be the result of fractionation of δ^{56}Fe towards the top of the OMZ, although that would be expected to shift values to heavier δ^{56}Fe (Section 3.1.2), or might point to a second source of light Fe. This source might also be from the Californian Margin or could be related to NPIW, which is present at 500 m depths at SAFe.

The light δ^{56}Fe signature observed associated with NPIW at SAFe could originate in the northern North Pacific source regions for NPIW, as appears to be the case for Zn* and Cd* (see Sections 3.2–3.3). Although δ^{56}Fe data has not been previously reported for NPIW, this low-salinity water mass corresponds to high Fe concentrations at ~500 m in the North Western Pacific (1–1.5 nmol kg^{-1}; Nishioka et al., 2007). These high Fe concentrations were attributed to ventilation of high-Fe intermediate depth waters in the surface sub-polar regions where NPIW is formed in the Okhotsk Sea and the Oyashio Region, and lateral transport within NPIW (Talley, 1993; Nishioka et al., 2007). Given that these high Fe concentrations are likely sourced from the Asian margin and carried in low-oxygen waters (Nishioka et al., 2007), this Fe might carry a light δ^{56}Fe signature from reducing sediments as observed in the North Atlantic OMZ (Conway and John, 2014a). If NPIW does carry a pre-formed δ^{56}Fe signal, this would be remarkable because it would suggest that a distal Asian shelf or sub-polar source contributes Fe to the surface ocean in the subtropical North East Pacific. It would also add weight to the idea that non-aeolian sources and light δ^{56}Fe signatures can be transported over long distances (~6000 km), despite the dynamic nature of the Fe cycle. In the North Pacific, the relative absence of isotopically heavy Fe sources such as dust could facilitate the transport of light δ^{56}Fe signatures over even greater distances than in the Atlantic.

Whichever source is responsible for the isotopically lighter δ^{56}Fe at 500 and 1500 m, the heavier δ^{56}Fe values at 750–1000 m probably reflect mixing of Fe sources with a pre-formed δ^{56}Fe signature carried with AAIW (600–1300 m) from the South Pacific. δ^{56}Fe data in AAIW from ~20°S showed this water mass to be -0.1‰ (Fitzsimmons et al., 2013), which is heavier than the water column at SAFe. The range of δ^{56}Fe values observed between 750 and 1000 m could therefore reflect mixing of light Fe from NPIW (-0.6‰) with AAIW since these two water masses are mixed in this depth interval (Talley et al., 2011), and/or mixing of background Fe from AAIW with Fe advected from the Californian margin at depths of ~800–1600 m. Higher spatial resolution δ^{56}Fe data would be necessary to distinguish these possibilities.

3.1.5. Fe sources below 2000 m and water column synthesis

Below 2000 m, δ^{56}Fe returns to heavier values, near -0.1‰ in PDW/UDCDW at 2000–3000 m and $+0.15 \pm 0.07$‰ to $+0.18 \pm 0.07$‰ in LCDW below 3000 m (Fig. 2a). This increase in δ^{56}Fe values with depth corresponds to declining Fe concentrations, reflecting both the lessening influence of horizontally transported sedimentary or hydrothermal Fe, and the influence of scavenging on Fe concentrations in older water. Indeed, LCDW are some of the oldest waters in the world, and the heavier δ^{56}Fe values ($+0.2$‰) here are close to crustal ($+0.09$‰; Beard et al., 2003), suggestive of Fe sourced from 'non-reductive' release from sediments or in apparent equilibrium with crustal δ^{56}Fe values (0 to $+0.3$‰; Radic et al., 2011; Homoky et al., 2013; Conway and John, 2014a; Labatut et al., 2014).

In evaluating the overall sources of Fe to the water-column at SAFe, therefore, we infer that Fe from reductive sediments is most important at intermediate depths of 500–2000 m, probably due to lateral transport of Fe from the Californian Margin through the North Pacific OMZ, with possible addition from NPIW. Vertical upwelling of light Fe from the OMZ horizon, together with mineral dust deposition at the surface, can explain heavier δ^{56}Fe in surface waters above 200 m, although here δ^{56}Fe signatures may be complicated by a range of other processes. Below the OMZ, Fe in deep waters (>4000 m) is likely sourced from contact with oxic sediments, while it is not yet clear from the available data whether lighter than crustal δ^{56}Fe values in PDW/UCDW (1500–4000 m) reflect a reduced sedimentary or very distal hydrothermal signal. Overall, δ^{56}Fe data from SAFe point to sedimentary margins being the dominant Fe sources in this region of the North Pacific, in agreement with both recent modeling efforts and δ^{56}Fe measurements from ferromanganese crusts which suggest that deep sedimentary or hydrothermal Fe sources may have dominated the deep Pacific Fe reservoir over the last ~80 million years (Chu et al., 2006; Horner et al., 2014; Tagliabue et al., 2014).

3.2. Cd and δ^{114}Cd at SAFe

The dissolved Cd concentration profile at SAFe (Fig. 3a) is typical for Cd in the North Pacific (e.g. Bruland, 1980). Dissolved Cd is characterised by low concentrations (<20 pmol kg^{-1}) at the surface, increasing rapidly with depth to a subsurface maximum of ~1040 pmol kg^{-1} at

1000 m (associated with AAIW). Below 1000 m, Cd concentrations are slightly lower in deep waters dominated by UCDW/PDW and LCDW (860–920 pmol kg^{-1}). At SAFe δ^{114}Cd is remarkably homogenous at depths of 500 m and below (Fig. 3a; mean $0.32 \pm 0.04‰$; 2SD $n = 8$). δ^{114}Cd from 1000 m in this study from 2009 ($+0.31 \pm 0.04‰$, 2σ) are consistent with our previous measurements of δ^{114}Cd in SAFe D1 and D2 standards from 1000 m that were collected in 2004 (mean $+ 0.26 \pm 0.02‰$, 2SD, $n = 5$; Conway et al., 2013). Above 500 m, δ^{114}Cd increases from $+0.30 \pm 0.04‰$ at 500 m to $+0.78 \pm 0.08‰$ at 200 m, as Cd concentrations decline from 800 to 138 pmol kg^{-1}. In the surface ocean above 200 m, δ^{114}Cd increases to even heavier values (+3‰) as Cd concentrations become very depleted due to biological uptake within the euphotic zone. Here, biological incorporation of light Cd into phytoplankton leaves the residual dissolved Cd pool isotopically heavy, with the very heavy δ^{114}Cd surface values consistent with previously reported values of +3 to +5‰ for similar low concentration surface waters in the Pacific and Atlantic (Ripperger et al., 2007; Conway and John, 2015).

The overall pattern in Cd and δ^{114}Cd reflects what is known about dissolved Cd and δ^{114}Cd in the oceans, namely that both are controlled by large-scale water mass circulation and influenced by biological activity in surface waters (e.g. Ripperger et al., 2007; Abouchami et al., 2014). A range of studies from different oceans now show δ^{114}Cd to be fairly homogenous (+0.2 to +0.3‰) in deep waters with Cd concentrations of 0.4–1 nmol kg^{-1} from the Pacific, Southern and Atlantic Oceans and the South China Sea (Ripperger et al., 2007; Boyle et al., 2012; Xue et al., 2012; Yang et al., 2012; Conway et al., 2013; Abouchami et al., 2014). We represent this deep-water δ^{114}Cd value as a purple dashed line in Fig. 3a (~+0.3‰). Biological uptake and incomplete regeneration, either *in situ* or via advection of preformed water-mass signals are responsible for higher δ^{114}Cd values in surface waters (<500 m) or through the intermediate depth Atlantic (Abouchami et al., 2014; Conway and John, 2015). The vertical gradients in Cd and δ^{114}Cd observed at SAFe above 500 m are most likely the result of a combination of biological uptake of light Cd in the euphotic zone, together with deeper regeneration and vertical upward mixing of deep waters. It is possible horizontal advection of nutrient-depleted surface water masses could also contribute to heavier δ^{114}Cd above 500 m.

Consistent with the now-widely known global Cd/PO_4^{3-} relationship, dissolved Cd and PO_4^{3-} profiles at SAFe are very similar (Fig. 3a). Indeed, the North East Pacific was the focus of some of the first studies that demonstrated the strong global correlation between these two elements (Boyle et al., 1976; Bruland et al., 1978a; Bruland, 1980), with the large scale distribution of both elements being broadly controlled by the same physical and biological factors. Despite the strong similarity between the marine distributions of dissolved Cd and dissolved PO_4^{3-}, processes that add or remove PO_4^{3-} or Cd from the oceans can cause small variations in Cd/PO_4^{3-} and Cd^*. Variability in the degree of uptake and regeneration of Cd and PO_4^{3-} in surface waters that set the pre-formed Cd/PO_4^{3-} of water masses, and local removal of Cd can both influence Cd/PO_4^{3-} and Cd^* (Baars et al., 2014; Janssen et al., 2014).

Recent data from Line P, in the sub-arctic Pacific, showed a negative Cd^* (−0.1) associated with the top of low-oxygen waters, attributed to the *in situ* removal of Cd from the water column as CdS (Janssen et al., 2014). At SAFe, a similar excursion to negative Cd^* is seen associated with the top of the OMZ, with Cd^* values reaching −0.12 at 750 m where dissolved oxygen is ~10 μmol kg^{-1}. This is supportive of the idea of water column removal of Cd associated with the onset of low-oxygen conditions, as previously hypothesized for both the North Pacific and North Atlantic (Janssen et al., 2014; Conway and John, 2015). In fact, at 750 m, the difference in Cd and PO_4^{3-} can also be clearly observed in the shape of the two profiles (Fig. 3a). It has been suggested that dissolved Cd is removed as isotopically light Cd sulfides within low-oxygen, but not anoxic, open ocean waters (Janssen et al., 2014), and recently it was shown that in the North Atlantic this leaves the residual dissolved Cd isotopically heavy (John and Conway, 2014). At SAFe, however, there is no evidence of any change in dissolved δ^{114}Cd associated with the Cd^* signal. This may be because the isotope fractionation associated with sulfide formation is small, or that the relative removal of Cd in the North Pacific is less than in the North Atlantic.

The observed Cd^* excursions of around −0.1 at 500–1000 m at SAFe and at Line P in the North Pacific are smaller than Cd^* minima (−0.24 to −0.25) reported from the top (90 m depth; 45 μmol kg^{-1} oxygen) of the Mauritanian OMZ in the North Atlantic (Janssen et al., 2014; Conway and John, 2015), but are broadly comparable with the −0.05 to −0.15 Cd^* signal seen throughout North Atlantic low oxygen waters (Conway and John, 2015). Given that the North Pacific OMZ is characterized by a pronounced low oxygen horizon (~550–2000 m; Fig. 2b) with dissolved oxygen concentrations as low as 10 μmol kg^{-1}, it is perhaps surprising that a similarly large change in both δ^{114}Cd and Cd^* is not observed in the Pacific. However, there are several factors which may be responsible for this difference. First, Cd is supplied to the intermediate depth North Atlantic by Antarctic Intermediate Water (AAIW), which is slightly depleted in Cd relative to PO_4^{3-} compared to deep North Atlantic reference waters (AAIW Cd^* of −0.02 to −0.04; Conway and John, 2015), while the top of the OMZ at SAFe is influenced by NPIW with a Cd^* of −0.01 to +0.01. Second, the degree to which metal sulfides are removed may depend not only on dissolved oxygen concentrations, but also the availability of organic particle micro-environments in which metal sulfides may form (Janssen et al., 2014; Janssen and Cullen, 2015). Such environments may be more abundant in the Eastern North Atlantic where there is intense biological activity related to the Mauritanian Upwelling region. Additionally, organic particle concentrations are likely to be higher at the top of the Mauritanian OMZ at 100 m depth, compared to 750 m depth in the North Pacific, due to regeneration of organic matter with depth. Together, these factors may provide more

particulate micro-environments for metal sulfide formation in the North Atlantic. This in turn may facilitate a more dramatic effect on the dissolved Cd reservoir at the top of the shallow Mauritanian OMZ compared to a more subtle effect throughout the deeper North Pacific OMZ. However, despite the more subtle Cd^* signals in the North Pacific, the −0.12 Cd^* minimum at SAFe still corresponds to a dissolved Cd concentration (917 pmol kg^{-1}) which is 120 pmol kg^{-1} less than would be predicted (1040 pmol kg^{-1}) from a Cd^* of 0 based on deep water Cd/PO_4^{3-}. This suggests that CdS removal does have the potential to be an important process for the distribution and cycling of Cd in this region of the ocean, consistent with recent studies (Janssen et al., 2014; Conway and John, 2015).

In surface waters above 500 m, Cd^* is ~0 at the surface (25 m), perhaps reflecting near-quantitative uptake of both Cd and P, or simply water-mass differences. Deeper in the water column, within high-oxygen surface waters, Cd^* declines to −0.10 at 200 m and then returns to ~0 at 350 m. It is not yet clear what is causing this shape in surface Cd^*, although a similar feature is also observed at Line P (Janssen et al., 2014). The pattern could point to the differential regeneration of Cd and PO_4^{3-} in surface waters, or advection of a signal from another region of the ocean. Just above the OMZ, at 500 m, a profile maximum in Cd^* (+0.01) is observed associated with the presence of NPIW. This water-mass is slightly enriched in Cd with a Cd/PO_4^{3-} of 0.321 compared to the deep Pacific at SAFe (0.317), probably reflecting transport of a pre-formed Cd/PO_4^{3-} signature from the source regions of NPIW in the Okhotsk Sea (0.37; Abe, 2002).

3.3. Zn and $\delta^{66}Zn$ at SAFe

Dissolved Zn at SAFe and in the North Pacific has a similar profile to dissolved silicate (Fig. 3b, this study; Bruland et al., 1978b), with low concentrations in surface waters due to biological uptake and a gradual increase with depth, reaching a maximum of ~9 nmol kg^{-1} within PDW/UCDW (3000 m). Both Zn and Si reach their concentration maximum at a much deeper depth than Cd or P. Set against this broad pattern, Zn^* data indicates that NPIW at 500 m, and AAIW mixed with NPIW at 750 m are both characterized by higher Zn/Si than the deep ocean. As we described above, NPIW is characterized by high Cd/PO_4^{3-} and light $\delta^{56}Fe$, which in the latter case we hypothesize could be carried from reductive sediments in the NPIW source regions in the Sea of Okhotsk. It is possible that the higher Zn^* observed within NPIW at SAFe is a transported source signal with Zn entrained into NPIW close to the Asian margin, and carried with the water mass through the intermediate North Pacific. This idea is consistent with several recent studies which showed high Zn concentrations relative to Si within NPIW at Line P (Janssen and Cullen, 2015) and high concentrations of Zn in the sub-arctic source regions for NPIW (Sea of Okhotsk and Sea of Japan; Kim et al., 2015). It is certainly feasible that the Zn^* signal in NPIW could be a preformed water-mass signature, since preformed Zn^* appears to be a conservative tracer within the oceans (e.g. Wyatt et al., 2014). Data from several GEOTRACES sections have already shown that elevated Zn^* signals can be transported great distances. For example, Zn^* within Mediterranean Outflow water travels from 35°N at least as far as 17°N, and Zn^* within Upper Labrador Sea Water appears to travel even further (Conway and John, 2014b). Antarctic Zn^* water mass signals are also transported northward into the South Atlantic (Wyatt et al., 2014). We recently showed that margin sediments are sources of dissolved Zn (Conway and John, 2014b), an observation that is repeated for the Californian Margin in this study. Similarly, the slight source of Zn to NPIW could be sediments on the Asian margin, or a riverine or anthropogenic source of Zn from East Asia. Additionally, Kim et al. (2015) recently suggested that elevated Zn within NPIW source regions could be caused by atmospheric dust input to surface waters.

In the deep ocean at SAFe, below 500 m, $\delta^{66}Zn$ is quite homogenous (+0.45 ± 0.03 to +0.56 ± 0.03‰), close to the mean $\delta^{66}Zn$ of +0.50 ± 0.14‰ 2SD (2SE of 0.01, $n = 223$) of the global oceans ⩾1000 m, calculated from data obtained so far (means of 0.53 ± 0.14‰, 2SD $n = 21$, in Zhao et al. (2014), and 0.50 + 0.13‰, 2SD $n = 202$, in Conway and John (2014b)). Above 500 m, in contrast to $\delta^{114}Cd$, $\delta^{66}Zn$ gradually decreases upward from +0.5‰ to values as light as −0.05 ± 0.09‰ at 100 m and −0.15 ± 0.06‰ at 25 m. This pattern of increasing $\delta^{114}Cd$ and decreasing $\delta^{66}Zn$ towards the surface at SAFe is similar to recent water-column data from the North Atlantic, where these signals were attributed primarily to biological uptake (Cd), and scavenging (Zn), respectively (John and Conway, 2014). In the latter-case, the suggestion of a role for scavenging was based on the oceanographic patterns of Zn and $\delta^{66}Zn$, culture experiments demonstrating adsorption of heavy Zn to degrading phytoplankton and simple 1-dimensional modeling studies (Conway and John, 2014b; John and Conway, 2014). More recently, adsorption of isotopically heavy Zn to organic material has also been demonstrated in incubation experiments with biofilms (Coutard et al., 2014).

The pattern in $\delta^{66}Zn$ observed at SAFE is also similar to the two previous published studies of $\delta^{66}Zn$ from the North Pacific, which showed light values (−0.1 to +0.2‰) over the top 200–400 m and then an increase to deep ocean values of +0.5‰ below this (Bermin et al., 2006; John, 2007). Culture studies show that phytoplankton preferentially incorporate lighter Zn, a fact typically invoked to explain heavy $\delta^{66}Zn$ values in very surface waters in other oceans (e.g. up to +0.9‰; John et al., 2007a; Conway and John, 2014b). Indeed, in the North Atlantic, a decrease in $\delta^{66}Zn$ from the deep ocean towards the surface is often accompanied by an increase to heavier $\delta^{66}Zn$ values at the very surface. At SAFe, however, we do not have data for the very surface, so it is not clear if $\delta^{66}Zn$ moves to heavier values, although our recent $\delta^{66}Zn$ measurement in the SAFe S1 standard was slightly heavier (+0.16 ± 0.14‰, 2σ; Conway et al., 2013). The lightest $\delta^{66}Zn$ value at SAFe (25 m) is coincident with elevated Zn concentration (0.7 nmol kg^{-1}), and it is not clear if this represents very

shallow recycling of biogenic light Zn as has been suggested for the North Pacific (Vance et al., 2012), cells bursting on filters during collection, or contamination (although the latter would be expected to be +0.1 to +0.3‰; John et al., 2007b).

Despite the current global dataset for seawater dissolved δ^{66}Zn demonstrating the near-homogeneity of the deep ocean (>500 m) for δ^{66}Zn (Conway and John, 2014b; Zhao et al., 2014; this study), there does appear to be small variability, on the order of 0.1–0.2‰. This variability is thus close to, but outside of, the limits of 2σ uncertainty of deep ocean δ^{66}Zn data (~0.02–0.08‰; Conway and John, 2014b; Zhao et al., 2014). At SAFe, δ^{66}Zn values gradually increase with depth from the surface to a maximum of $+0.56 \pm 0.03$‰ (2σ) at 75–1000 m, and then decline to $+0.52 \pm 0.02$ to $+0.53 \pm 0.02$‰ (2σ) between 1500–3000 m and to $+0.46 \pm 0.02$‰ (2σ) within deeper waters. While this 0.1‰ offset in δ^{66}Zn at SAFe is close to the combined 2σ error on the data (0.04–0.06‰), the pattern hints at a profile shape that can also be observed in data from other oceans, where the shift to heavier values at mid-depths is larger. (Fig. 4; Conway and John, 2014b; Zhao et al., 2014). For example, we recently documented a mid-depth δ^{66}Zn maximum in the intermediate North Atlantic Ocean, with heavy δ^{66}Zn (up to +0.7‰) at intermediate depths of 750–2000 m at 7 stations in the eastern North Atlantic (Fig. 4; Fig. 8 of Conway and John, 2014b). With the recent publication of full water-column profiles of δ^{66}Zn from the South Atlantic, heavy δ^{66}Zn (+0.6 to +0.7‰) is also visible at intermediate depths of ~1000–3000 at two stations in the South Atlantic and at 3000–4000 m in one station in the South Atlantic (Zhao et al., 2014). In the one example where the mid-depth maximum is observed at deeper depths within Southern Ocean Station PS71-104-2 (Zhao et al., 2014), the heavier δ^{66}Zn values are present partially within LCDW, which is subducted from intermediate depths further south.

While these excursions to heavier δ^{66}Zn at intermediate depths in the North Atlantic, North Pacific and Southern Ocean are small in magnitude (~0.1 to 0.2‰), the values fall outside 2SE (and in some cases 2SD) of the calculated deep ocean mean δ^{66}Zn value. Additionally, the pattern is reproduced in different areas of the ocean by two independent laboratories, suggesting that this pattern may be a real feature of Zn biogeochemistry that is occurring at intermediate depths within the ocean. This tells us several things. Firstly, this pattern in δ^{66}Zn suggests that Zn is not behaving as a simple nutrient-type element, i.e. controlled just by water-mass circulation and biological uptake/regeneration. In contrast to δ^{66}Zn, both δ^{114}Cd and δ^{30}Si show simpler isotope profiles, with heavier values in surface ocean due to biological uptake, and large-scale distributions controlled by mixing of water masses with different 'biological' preformed signatures (de Souza et al., 2012a,b; Abouchami et al., 2014; Conway and John, 2015). Secondly, although some rivers have heavy dissolved δ^{66}Zn signatures, the overall δ^{66}Zn signature of external Zn inputs to the oceans is thought to be isotopically lighter than seawater (Little et al., 2014). This means that mid-depth excursions to heavier δ^{66}Zn values must be the result of fractionation

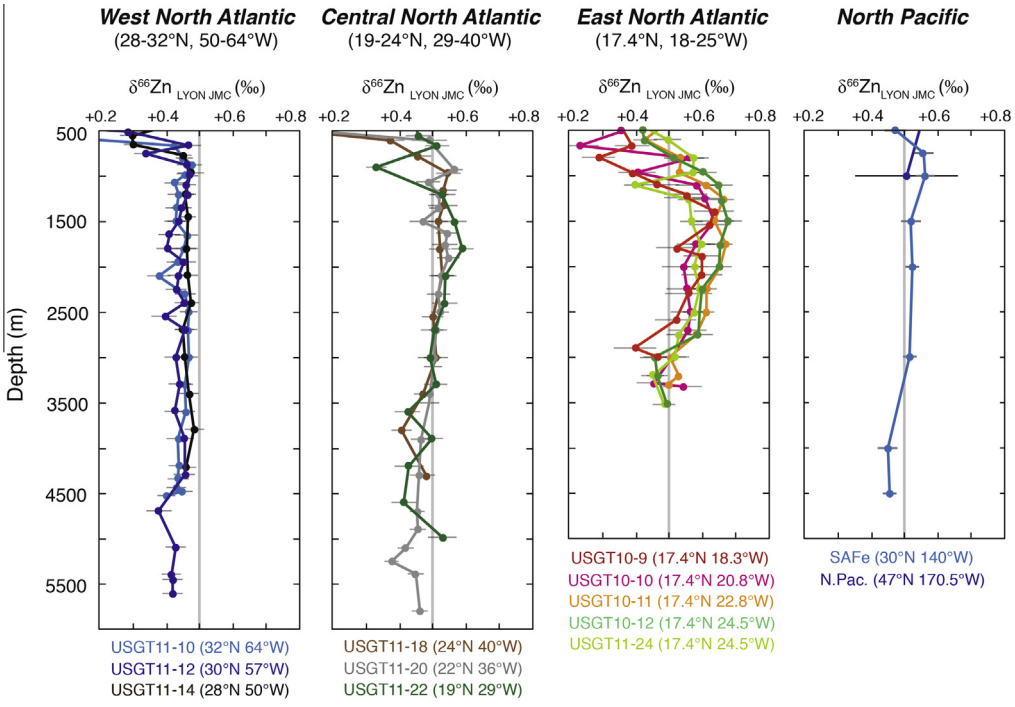

Fig. 4. Dissolved δ^{66}Zn profiles from the West North Atlantic, Central North Atlantic, East North Atlantic (Conway and John, 2014b) and North East Pacific (this study; John, 2007). The vertical grey bars represent our current best estimate of the δ^{66}Zn signature of the deep ocean Zn reservoir (+0.50‰) calculated from the data used to calculate deep ocean means by Conway and John (2014b; n = 202) and Zhao et al. (2014, n = 21). We reproduce error bars from their respective publications, with grey bars denoting either 2σ internal error, or 2SD of the mean (for the data of John (2007)). (For interpretation of colour in this figure, the reader is referred to the web version of this article.)

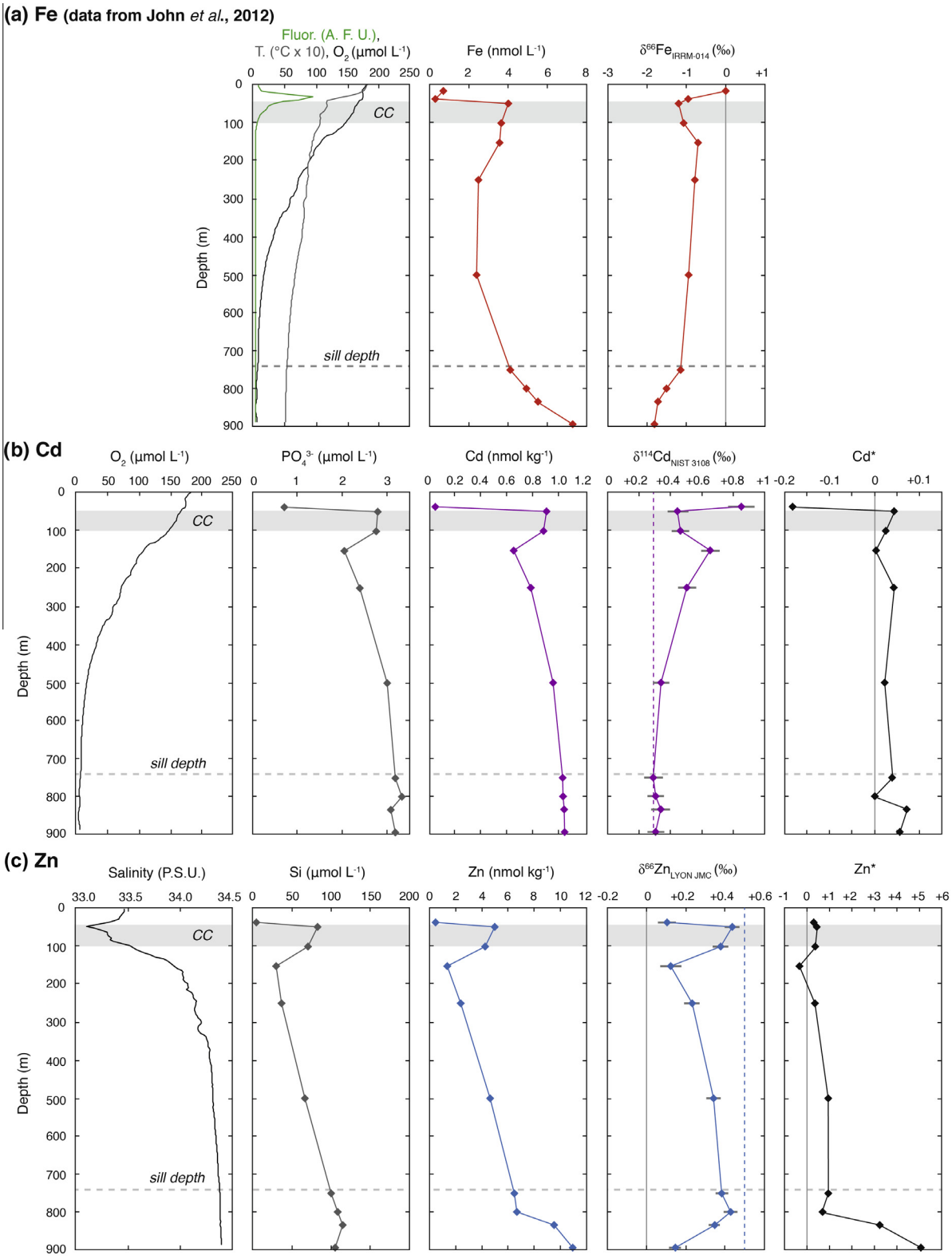

Fig. 5. Dissolved (a) Fe, (b) Cd and (c) Zn concentration and stable isotope ratio (δ^{56}Fe, δ^{114}Cd and δ^{66}Zn) profiles from the San Pedro Basin close to California (33.8°N 118.4°W), with supporting dissolved data. Fe concentration, δ^{56}Fe, oxygen, fluorescence and temperature are reproduced from John et al. (2012). All errors on isotope ratios are 2σ internal error as calculated in the text. Zn* and Cd* are calculated as in the text, with 0 marked as a vertical grey line. Sill depth is marked with a horizontal grey dashed line, deep ocean δ^{66}Zn and δ^{114}Cd signatures are denoted by the same vertical coloured dashed lines as in Fig. 3. The grey bar labeled CC marks the low-salinity horizon corresponding to the California Current at 50–100 m. (For interpretation of the references to colour in this figure legend, the reader is referred to the web version of this article.)

associated with internal cycling, such as the regeneration of a heavy adsorbed Zn phase or the removal of a light Zn phase such as Zn sulfides from the dissolved Zn reservoir (Conway and John, 2014b; John and Conway, 2014; Zhao et al., 2014).

In the South Atlantic profiles described by Zhao et al. (2014), in contrast to the North Atlantic, dissolved oxygen is always >150 μmol kg^{-1}, and so ZnS removal is not considered likely. In other areas of the oceans, where low-oxygen waters are present, the situation may not be as simple. A ZnS removal process has been recently proposed to explain a Zn deficit within low-oxygen waters within the North Pacific OMZ at Line P (Janssen and Cullen, 2015), analogous to that proposed for Cd (Janssen et al., 2014). This Zn deficit was observed at Line P as a subtle decoupling of Zn and Si at depths of 400–1000 m, with Zn concentrations decreasing, remaining stable, or increasing less than Si with depth through this horizon (Janssen and Cullen, 2015). At all 5 of the Line P stations, although especially closest to the coast, a 'bite' appeared to be missing from the Zn concentration depth profiles (Janssen and Cullen, 2015). At the SAFe station, by comparison, Zn and Si profiles look more similar (Fig. 3b). As a result, Zn^* at SAFe does not provide any clear evidence of ZnS removal, in contrast to Cd at SAFe (Fig. 3a; Section 3.2) or both Cd and Zn at Line P (Janssen et al., 2014; Janssen and Cullen, 2015). However, both the full Zn^* profile and Zn^* just above the OMZ (500 m depth) at SAFe are dominated by the positive Zn^* in NPIW (+1). It is possible this NPIW Zn^* signal could be obscuring negative Zn^* excursions at 750–1000 m associated with ZnS removal, which are observed at deeper depths (−0.1 to −0.3; 1500–2000 m). Additionally, the Zn deficit at Line P appeared to diminish along the transect away from the coast, suggesting that removal may depend on the greater availability of particle micro-environments near the coast (Janssen and Cullen, 2015). If this is the case, a Zn^* signal at SAFe might be expected to be much more subtle than at Line P, and could perhaps be overprinted by local processes such as scavenging and regeneration or mixing with other water masses.

In terms of $\delta^{66}Zn$ evidence, it is worth noting that the heaviest $\delta^{66}Zn$ values at SAFe correspond to the most negative Cd^* values, where it might be expected the strongest effect of ZnS removal on $\delta^{66}Zn$ would be observed (Fig. 3). This pattern is also consistent with the idea that ZnS removal would be expected to drive the resultant dissolved $\delta^{66}Zn$ to heavier values, as sulfide precipitation is expected to preferentially incorporate light Zn (Archer et al., 2004). Thus, ZnS removal remains a possible candidate for explaining the pattern in $\delta^{66}Zn$ at SAFe, alongside the idea of adsorption of heavy Zn within the subsurface ocean together with regeneration of this pool at intermediate depths (Conway and John, 2014b). Both processes are also possible candidates for the mid-depth $\delta^{66}Zn$ maxima in the Eastern North Atlantic, although this is located below the Mauritanian OMZ (Conway and John, 2014b). Thus, at present we cannot conclusively say whether ZnS removal or regeneration of an adsorbed phase, or a combination of the two, might be responsible for the observed mid-depth maximum observed in seawater $\delta^{66}Zn$ profiles (Conway and John, 2014b; this study; Fig. 4). However, the fact that heavier mid-depth $\delta^{66}Zn$ maxima have also been observed in the Southern Ocean (Zhao et al., 2014), where oxygen is not low, would seem to at least provide supporting evidence for the hypothesis that adsorption and regeneration of Zn plays a global role in the deeper regeneration of Zn compared to other nutrients (John and Conway, 2014).

Lastly, we note that the lighter $\delta^{66}Zn$ values of deepest waters (within LCDW) at SAFe are slightly lighter (+0.46‰), similar to the Western North Atlantic (close to +0.45‰; Conway and John, 2014b). Zn^* values are also slightly higher (Fig. 3b). This $\delta^{66}Zn$ value is subtly lighter than the deep ocean average published to date (+0.5‰; Conway and John, 2014b; Zhao et al., 2014). Although this may be due to uncertainty on measurements, it may also be because whole ocean mean calculations are biased by present coverage that favours intermediate depths. We suggest more coverage of the world's oceans for $\delta^{66}Zn$ is therefore necessary to establish an accurate deep ocean average $\delta^{66}Zn$ value (and its spatial variability), that will be important for future attempts to understand or model the overall ocean mass balance of Zn.

3.4. Cd, $\delta^{114}Cd$, Zn and $\delta^{66}Zn$ at San Pedro

The vertical profiles of both Zn and Cd concentrations and stable isotope ratios in the San Pedro basin (Fig. 5b and c) can be interpreted in the context of water-mass mixing, together with local processes such as biological activity and sediment interactions. With the exception of samples from 50 to 100 m depths, the profiles may be largely discussed in terms of vertical and local horizontal processes that fractionate $\delta^{114}Cd$ and $\delta^{66}Zn$ from deep ocean signatures of +0.5‰ ($\delta^{66}Zn$) and +0.3‰ ($\delta^{114}Cd$). The 50 and 100 m samples (grey bar, Fig. 5a–c) are strongly influenced by the southward flow of the low salinity California Current system waters (CC; ~33–33.4 p.s.u; King and Barbeau, 2011). At these southerly latitudes the low-salinity California Current has a subsurface core at depths of 50–100 m, can travel close to the coast (<10 km) and recirculates at these depths through the South California Bight (Lynn and Simpson, 1987; Reid et al., 1958). The California Current system provides variable upwelling of nutrients and trace metals to the surface mixed layer along the Californian margin, dependent on local upwelling and mesoscale eddies (King and Barbeau, 2011; Biller and Bruland, 2014). Thus, the California Current is likely to sporadically carry high concentrations of nutrients and trace-metals to the San Pedro water-column, overprinting local processes. We therefore discuss these two parts of the profiles separately; first, we discuss the vertical profiles without the samples from 50–100 m, and then consider the two samples from 50 and 100 m separately.

At San Pedro, Cd concentrations decrease from a maximum of 1040 pmol kg^{-1} at 900 m in the deep basin, to much lower concentrations in surface waters (40 pmol kg^{-1} at 35 m), very similar to the concentrations observed at the

open-ocean SAFe station. As at SAFe, $\delta^{114}Cd$ is close to +0.3‰ below 500 m, with an increase in $\delta^{114}Cd$ towards heavier values in surface waters (+0.85 ± 0.08‰ at 35 m), indicative of the influence of biological uptake and regeneration of Cd in shallower waters. With the exception of the 35 m sample, dissolved Cd and PO_4^{3-} profiles show similarity throughout the water column, with Cd^* values ranging from +0.00 to +0.07. It is not clear what causes the slight fluctuations in Cd^*, but the smaller values at 35 m and 800 m are associated with fluctuations in PO_4^{3-}, perhaps pointing to an external source of phosphate from sediments at these depths. Despite the low-oxygen concentrations (<75 μmol L^{-1}) present below 200 m of the San Pedro water column, and the evidence for CdS precipitation at open-ocean North Pacific sites (this study; Janssen et al., 2014), there is less clear Cd^* or $\delta^{114}Cd$ evidence for *in situ* CdS precipitation within the water column at San Pedro, when compared to SAFe or Line P. As discussed in Section 3.2, in both the North Atlantic and North East Pacific, a negative Cd^* signal is seen largely associated with the top of low-oxygen waters (this study; Janssen et al., 2014; Conway and John, 2015), suggesting that another factor such as the presence of high concentrations of biological particles is facilitating Cd removal as CdS in micro-environments (Conway and John, 2015; Janssen and Cullen, 2015). It could be that there are not sufficient quantities of these particles at intermediate depths (150–200 m) in the San Pedro basin, or that a Cd^* signal is largely obscured by the northward movement of the Californian Undercurrent at these depths (Talley et al., 2011). However, it should be noted that a small minimum in Cd^* (+0.00) and a pronounced minimum in Zn^* (−0.3) are both observed at ~150 m where dissolved oxygen drops below 100 μmol L^{-1}. These provide possible evidence for small water-column loss of both Cd and Zn due to sulfide formation as oxygen concentrations decline.

The distribution of dissolved Zn in the San Pedro basin, in contrast to Cd, cannot simply be interpreted in the context of biological uptake and regeneration. Zn concentrations at ~800 m are similar to that observed at SAFe (6.7 vs 6.62 nmol kg^{-1}), and decrease towards the surface. However, $\delta^{66}Zn$ values are always lighter than 'oceanographic' (~+0.5‰, dashed blue line), with the heaviest values at 800 m (+0.43 ± 0.03‰), and decreasing towards the surface (+0.11 ± 0.05‰ at 35 m). This could reflect the influence of adsorption of Zn to organic matter, which has been suggested for the North Atlantic and at SAFe (this study; John and Conway, 2014). The muted excursion to lighter $\delta^{66}Zn$ values towards the surface in San Pedro compared to the SAFe station (+0.11 ± 0.05 vs. −0.15 ± 0.06‰) could also be explained by lower organic particle availability. Between 150 and 500 m, Zn^* and $\delta^{66}Zn$ profiles have a similar shape, supporting the idea that heavy Zn is being removed from the water column by scavenging. Below this, the opposite shape of the Zn and $\delta^{66}Zn$ profiles suggests that addition of isotopically light Zn is causing the pattern in both Zn^* and $\delta^{66}Zn$. As has been documented for Fe in the San Pedro (John et al., 2012), this source is likely to be margin sediments. In fact, with the exception of 150 m, Zn^* values are elevated throughout the top 800 m (+0.3 to +1), indicative of a 'non-oceanographic' (i.e. not with a Zn/Si ratio of 0.056 and a $\delta^{66}Zn$ of +0.5‰) source of Zn throughout the water column at San Pedro.

Both adsorption/removal of heavy Zn and addition of sedimentary Zn are likely to be occurring to different degrees throughout the full water column at San Pedro, complicating efforts to use $\delta^{66}Zn$ alone to fully constrain processes. However, within the silled basin below 800 m, dissolved Zn concentrations increase dramatically from ~7 nmol kg^{-1} at 800 m to 11 nmol kg^{-1} at 900 m, coupled with a decrease in $\delta^{66}Zn$ from +0.43 ± 0.03 to +0.15 ± 0.03‰ and a large excursion in Zn^* (to +5). The absence of enhanced dissolved silicate concentrations at these depths indicates that this Zn is 'non-oceanographic', i.e. not sourced from deeper nutrient-rich waters, and is consistent with a flux of isotopically light Zn from sediments. This release of Zn is similar to that described for dissolved Fe in the San Pedro, with vertical transport of Fe from reduced sedimentary pore-water in benthic sediments thought to dominate the water column below the basin sill depth (John et al., 2012). If we simply assume that the increase in Zn between 800 and 895 m (+4.2 nmol kg^{-1}) and the decline in $\delta^{66}Zn$ (+0.44 to +0.15‰) is caused by addition of sedimentary Zn we can use these differences in Zn and $\delta^{66}Zn$ and a simple two component isotope mass balance equation (Eq. (4)) to approximate the $\delta^{66}Zn$ signature of the sedimentary Zn. This calculation generates a sedimentary $\delta^{66}Zn$ signature of −0.3‰, which is lighter than known values of crustal, anthropogenic and bulk sediment Zn under various redox conditions (+0.1 to +0.3‰; Maréchal et al., 2000; Archer et al., 2004; Chapman et al., 2006; John et al., 2007b; Little et al., 2014).

The form and mechanism of release of this sedimentary Zn is still unknown, as a pore-water or sedimentary release of Zn has not yet been characterized *in situ* within sediments. However, the light $\delta^{66}Zn$ signatures inferred for San Pedro sediment release are similar to $\delta^{66}Zn$ inferred for both oxic and reductive margins in the North Atlantic ($\delta^{66}Zn$ of −0.5 to −0.8‰; Conway and John, 2014b). There, we suggested one explanation for such light $\delta^{66}Zn$ values could be the release of biogenic Zn from sediments. This could also be the source of light $\delta^{66}Zn$ release at San Pedro. Alternatively, dissolution of Zn sulfides, which would be expected to be isotopically light (Archer et al., 2004), could be a source of Zn to the water column. These Zn sulfides could have formed in anoxic sediments and then perhaps be redissolved or remobilized as colloids (<0.2 μm) as the deep basin is periodically flushed by higher oxygen water (John et al., 2012).

Future sedimentary studies will be required to investigate the mechanism by which Zn is released from ocean floor sediments to the water column, as well as for characterizing the chemical form of this 'dissolved Zn'. Nevertheless, despite a lack of understanding of the mechanism by which this Zn might be released, it is clear from water-column data that margin sediments can be large local sources of Zn under both low and high oxygen conditions (this study; Conway and John, 2014b). It is also clear that sediments in these environments are sources of both Zn

and Fe, but not of dissolved Cd. While there is insufficient spatial data to constrain how widespread Zn release might be on the Southern Californian Margin, or whether dissolved Zn released from sediments is transported out into the open-ocean, distal transport is plausible. Other studies provide some insight into how margin sediments might influence phytoplankton in the open ocean, showing elevated dissolved Fe in the surface mixed layer and water-column off California, attributed to a benthic Fe supply (e.g. Bruland et al., 2001). Similarly, recent work from central California demonstrate a supply of trace metals (Mn, Fe, Co, Cu) from benthic sediments to the Californian Current system (Biller and Bruland, 2013), although they found no substantial addition of dissolved Zn or Cd. Perhaps consistent with that study, the very elevated Zn^* values at San Pedro are confined to the deep silled basin. However, Zn^* values of +0.3 can be observed throughout the water column, including within the Californian Current (see below), suggesting a small, but observable, contribution of Zn from sediments.

For the two samples at 50–100 m depth, we observe elevated dissolved concentration of Zn (4–5 nmol kg^{-1}), Cd (900 pmol kg^{-1}), Si (70–80 nmol L^{-1}) and PO_4^{3-} (2.8 nmol L^{-1}) associated with low salinity (33.2–33.4 p.s.u). This low-temperature, low-salinity (<33.4 p.s.u.) water at shallow depths is characteristic of the southward flowing California Current along the Californian coast (Lynn and Simpson, 1987; King and Barbeau, 2011) which recirculates through the South California Bight at these depths (Reid, 1958). The elevated nutrient concentrations, together with deeper-water signatures of both $\delta^{66}Zn$ (+0.4‰) and $\delta^{114}Cd$ (+0.4‰), are suggestive of upwelling of deeper water to the 50–100 m layer, associated with Ekman and sporadic eddy-driven upwelling on the Californian Margin (Talley et al., 2011). Dissolved Fe concentrations at 50–200 m are also elevated (4 nmol L^{-1}), and isotopically light ($\delta^{56}Fe$ near −1.2‰; John et al., 2012), also suggestive of upwelling of deep water with a sedimentary Fe source.

An alternative explanation for the two errant data points could be that bottles were tripped at the wrong depth, and we can use data from the three elements to consider that possibility. Of the three isotope systems, $\delta^{114}Cd$ is most simply affected by biological uptake and regeneration, leading to a vertical monotonic increase towards the surface, and so is most diagnostic for establishing the depth of upwelled water. A dissolved Cd concentration of 900 pmol kg^{-1} and a $\delta^{114}Cd$ of +0.4‰ are similar to ~350 m depth waters at the SAFe station. However, the $\delta^{66}Zn$ and $\delta^{56}Fe$ signals, as well as Fe and Zn concentrations, would indicate much deeper depths of around ~750 m. The data are therefore inconsistent with the samples being from a deeper depth in the San Pedro water column, and so we can discount the idea that bottles were mis-tripped. Of course, this consideration also means that the elevated concentrations are unlikely to be the result of *in-situ* upwelling within the San Pedro basin itself. Instead, the signals may arise from upwelled deep water from further north that has been laterally advected into the San Pedro basin with the California Current. One possibility for the source of the metals at shallower depths is the Santa Barbara Basin (560 m deep), which is located just to the North West of the San Pedro (Fig. 1a), and where much higher concentrations of Fe (4–6 nmol L^{-1}) and low $\delta^{56}Fe$ signatures (~−1‰) have been documented at depths of 300–400 m (John et al., 2012). Sporadic eddy-driven upwelling from depths of several hundred meters is in fact typical of the California current system, with the southern region (32–36°N) showing strongest upwelling through the summer and as late as September, when these samples were collected (Talley et al., 2011).

Data from San Pedro adds weight to the idea that Fe from reductive sediments may be upwelled and carried laterally within the California current systems along the margin, providing a source of Fe to phytoplankton outside these basins, as has been suggested throughout the Californian Current system (King and Barbeau, 2011; Biller and Bruland, 2013, 2014). Additionally, elevated Zn^* in the two samples from the Californian Current suggests that a sedimentary Zn source is also present at locations further North along the Californian margin and more widespread than just the San Pedro basin, though such a signal was not observed in data from Central California (Biller and Bruland, 2013). Low oxygen sediments along the margin are therefore potentially a source of not just Fe to the Southern California Current system (e.g. Johnson et al., 1999), but also Zn as well. Globally, sediments under low-oxygen waters may be important sources of Zn in other regions with similar hydrography to the Californian Current System, or where anoxic basins are periodically flushed with higher-oxygen waters.

4. CONCLUDING REMARKS AND BASIN-WIDE SYNTHESIS

We have presented two multiple-isotope ($\delta^{56}Fe$, $\delta^{66}Zn$ and $\delta^{114}Cd$) profiles for the North Pacific, one from the SAFe station in the open-ocean subtropical North East Pacific and another from the San Pedro marginal basin on the Californian margin. These data represent, to our knowledge, the first full-water column profiles for $\delta^{66}Zn$ and $\delta^{56}Fe$ profile from the open-ocean North Pacific and the first observations of dissolved $\delta^{66}Zn$ and $\delta^{114}Cd$ in a low-oxygen marginal basin.

At the basin scale, these data have allowed us to provide insights into the differing cycles of Fe, Zn and Cd in the North Pacific Ocean. At SAFe, data suggests that the Fe budget over the top 2000 m is dominated by isotopically light dissolved $\delta^{56}Fe$, which we suggest points to lateral transport and mixing of sedimentary Fe from reduced Californian margin sediments through the pronounced North Pacific Oxygen Minimum Zone (~550–2000 m depth). This idea is consistent with studies showing a plume of higher dissolved Fe concentration extending ~2000 km from the Californian Margin to SAFe, and the very isotopically light signature of pore-waters and water-column $\delta^{56}Fe$ along the North American margin including the San Pedro basin (Johnson et al., 1997; Severmann et al., 2010; John et al., 2012). While the possible influence of hydrothermal Fe at intermediate depths at SAFe is not apparent from

δ^{56}Fe data, we cannot discount the possibility that hydrothermal Fe is present at SAFe with a δ^{56}Fe signature similar to other Fe sources which are present at the same depths. Heavier values (~+0.2‰) in deep waters (below <4000 m) are consistent with a non-reductive sedimentary source of Fe. In general, the much lighter δ^{56}Fe observed in the North Pacific, compared to the North Atlantic, supports our previous attribution of isotopically heavy Fe to dust in the North Atlantic, and is consistent with the emerging consensus that aeolian dust deposition is not the only important source of Fe to the global ocean. Our data also provide support for the idea that δ^{56}Fe source signatures may be maintained over great distances and can therefore be used to provide a useful tool for tracing sources of Fe through the ocean.

At 500 m depth, where oxygen is slightly higher than within the OMZ (100 μmol kg^{-1}), North Pacific Intermediate Water carries a very light δ^{56}Fe signature (−0.6‰), which could point to an additional reduced sedimentary input in NPIW source regions. Cd^* and Zn^* are also distinctive in this water mass, highlighting the potential importance of processes in NPIW source regions for the distribution of these trace metals at shallow depths (⩽500 m) in the North Pacific. At the broad scale, consistent with current knowledge, data from both SAFe and San Pedro suggests that the distribution of both Cd and Zn in the North Pacific are most strongly influenced by water-mass circulation, with biological uptake/regeneration in surface waters <500 m. δ^{114}Cd at both locations is characterized by a deep water signature (~+0.3‰) below 500 m, and fractionation towards heavier values in surface waters, attributed to biological uptake of light Cd into phytoplankton. Set against this overall pattern, however, low-oxygen waters may play a small additional role in the regional distribution of Cd. Negative Cd^* values within the Pacific OMZ at SAFe (750–2000 m) are suggestive of a water-column removal process of dissolved Cd as Cd sulfides, supporting recent studies that suggest that precipitation of CdS in low-oxygen waters may be an important worldwide process for the marine Cd budget (Janssen et al., 2014). A lack of correspondingly strong evidence for CdS in low-oxygen waters at San Pedro may be related to the availability of suitable organic particulate micro-environments, but also highlights the fact that the metal sulfide removal hypothesis is not yet completely understood.

Zn, by comparison to Cd, is more complicated, with several additional processes likely to be affecting the distribution of Zn and δ^{66}Zn at both locations. At SAFe, light δ^{66}Zn in surface waters <500 m, and a small mid-depth δ^{66}Zn maximum at 750–1000 m set against a deep water δ^{66}Zn value of +0.5‰ provide further evidence for the hypothesis that scavenging of heavy Zn in the subsurface and regeneration of this at intermediate depths may be influencing the vertical distribution of Zn in the oceans. These processes may help to explain the silicate-like deeper-regeneration of Zn in the oceans. Evidence for the idea that Zn precipitates as ZnS in low-oxygen waters (Janssen and Cullen, 2015) is scant at both locations in this study, but remains a possibility that could also be invoked to explain mid-depth heavier δ^{66}Zn at SAFe. Lastly, Zn^* and δ^{66}Zn data from San Pedro show that dissolved Zn in the deep silled basin is strongly affected by the addition of light Zn from low-oxygen sediments, as has previously been shown for Fe (John et al., 2012). Sporadic eddy-driven upwelling of water from deep waters in these restricted Californian basins may therefore provide a source of Zn, as well as Fe, to surface waters both from deep water and margin sediments. It is also interesting to note that there is no corresponding evidence for Cd release from sediments, a pattern repeated in the North Atlantic where both oxic and reductive sediments are sources of Zn and Fe but not Cd (Conway and John, 2014a,b, 2015). Like Fe, Zn may potentially be carried within the surface California Current along the North American Margin or into the North Pacific, with potential implications for patterns of primary productivity. Although, there is no evidence of Californian sedimentary-margin Zn reaching the SAFe station, we do find elevated Zn^* (+1) in NPIW at SAFe which suggests that sedimentary Zn can be transported over long distances and may be an important consideration for the oceanic Zn cycle.

ACKNOWLEDGEMENTS

The data presented in this study are available as Supplementary Data. We thank the Chief Scientists, Captain, crew and clean sampling team on board GEOTRACES IC2 in the North Pacific, including those who measured nutrients, salinity, temperature and oxygen. We also thank J. Mendez, J. Moffett and J. Adkins for their involvement in the original collection of the San Pedro Basin water samples used in this study, A. Rosenberg for technical assistance at USC, J. Fitzsimmons for useful discussion about Pacific Fe and water masses, and C. Benitez-Nelson for providing San Pedro dissolved nutrient data. We also appreciated the insightful comments made by two anonymous reviewers and Associate Editor Claudine Stirling, which helped us to refine our thinking and improve this manuscript. This study was funded by NSF Grant OCE-1235150.

APPENDIX A. SUPPLEMENTARY DATA

Supplementary data associated with this article can be found, in the online version, at http://dx.doi.org/10.1016/j.gca.2015.05.023.

REFERENCES

Abe K. (2002) Preformed Cd and PO_4 and the relationship between the two elements in the northwestern Pacific and the Okhotsk Sea. *Mar. Chem.* **79**, 27–36. http://dx.doi.org/10.1016/S0304-4203(02)00038-5.

Abouchami W., Galer S. J. G., de Baar H. J. W., Middag R., Vance D., Zhao Y., Klunder M., Mezger K., Feldmann H. and Andreae M. O. (2014) Biogeochemical cycling of cadmium isotopes in the Southern Ocean along the Zero Meridian. *Geochim. Cosmochim. Acta* **127**, 348–367. http://dx.doi.org/10.1016/S0304-4203(02)00038-5.

Archer D. E. and Johnson K. (2000) A model of the iron cycle in the ocean. *Global Biogeochem. Cycles* **14**, 269–279. http://dx.doi.org/10.1029/1999GB900053.

Archer C., Vance D. and Butler I. B. (2004) Abiotic Zn isotope fractionations associated with ZnS precipitation. *Geochim. Cosmochim. Acta* **68**. http://dx.doi.org/10.1016/j.gca.2004.05.008. A325-A325.

Aumont O., Maier-Reimer E., Blain S. and Monfray P. (2003) An ecosystem model of the global ocean including Fe, Si, P colimitations. *Global Biogeochem. Cycles* **17**, 1060. http://dx.doi.org/10.1029/2001GB001745.

Baars O., Abouchami W., Galer S. J. G., Boye M. and Croot P. L. (2014) Dissolved cadmium in the Southern Ocean: distribution, speciation, and relation to phosphate. *Limnol. Oceanogr.* **59**, 385–399. http://dx.doi.org/10.4319/lo.2014.59.2.0385.

Beard B. L., Johnson C. M., Von Damm K. L. and Poulson R. L. (2003) Iron isotope constraints on Fe cycling and mass balance in oxygenated Earth oceans. *Geology* **31**, 629–632. http://dx.doi.org/10.1130/0091-7613(2003)031%3C0629:IICOFC%3E2.0.CO;2.

Bennett S. A., Rouxel O. J., Schmidt K., Garbe-Schonberg D., Statham P. J. and German C. R. (2009) Iron isotope fractionation in a buoyant hydrothermal plume, 5°S Mid-Atlantic Ridge. *Geochim. Cosmochim. Acta* **73**, 5619–5634. http://dx.doi.org/10.1016/j.gca.2009.06.027.

Bermin J., Vance D., Archer C. and Statham P. J. (2006) The determination of the isotopic composition of Cu and Zn in seawater. *Chem. Geol.* **226**, 280–297. http://dx.doi.org/10.1016/j.chemgeo.2005.09.025.

Biller D. V. and Bruland K. W. (2013) Sources and distributions of Mn, Fe Co, Ni, Cu, Zn, and Cd relative to macronutrients along the central California coast during the spring and summer upwelling season. *Mar. Chem.* **155**, 50–70. http://dx.doi.org/10.1016/j.chemgeo.2005.09.025.

Biller D. V. and Bruland K. W. (2014) The central California Current transition zone: a broad region exhibiting evidence for iron limitation. *Prog. Oceanogr.* **120**, 370–382. http://dx.doi.org/10.1016/j.pocean.2013.11.002.

Boyle E. A. and Jenkins W. J. (2008) Hydrothermal iron in the deep western South Pacific. *Geochim. Cosmochim. Acta* **72**, A107.

Boyle E. A., Sclater F. and Edmond J. M. (1976) On the marine geochemistry of cadmium. *Nature* **263**, 42–44. http://dx.doi.org/10.1038/263042a0.

Boyle E. A., Bergquist B., Kayser R. A. and Mahowald N. M. (2005) Iron, manganese, and lead at Hawaii Ocean Time-series station ALOHA: temporal variability and an intermediate water hydrothermal plume. *Geochim. Cosmochim. Acta* **69**, 933–952. http://dx.doi.org/10.1016/j.gca.2004.07.034.

Boyle E. A., John S. G., Abouchami W., Adkins J. F., Echegoyen-Sanz Y., Ellwood M. J., Flegal A. R., Fornace K., Gallon C. and Galer S. J. G. (2012) GEOTRACES IC1 (BATS) contamination-prone trace element isotopes Cd, Fe, Pb, Zn, Cu, and Mo intercalibration. *Limnol. Oceanogr. Methods* **10**, 653–665. http://dx.doi.org/10.4319/lom.2012.10.653.

Bruland K. W. (1980) Oceanographic distributions of cadmium, zinc, nickel, and copper in the North Pacific. *Earth Planet. Sci. Lett.* **47**, 176–198. http://dx.doi.org/10.1016/0012-821x(80)90035-7.

Bruland K. W., Knauer G. A. and Martin J. H. (1978a) Cadmium in northeast Pacific Waters. *Limnol. Oceanogr.* **23**, 618–625. http://dx.doi.org/10.4319/lo.1978.23.4.0618.

Bruland K. W., Knauer G. A. and Martin J. H. (1978b) Zinc in Northeast Pacific water. *Nature* **271**, 741–743. http://dx.doi.org/10.1038/271741a0.

Bruland K. W., Rue E. L. and Smith G. J. (2001) Iron and macronutrients in California coastal upwelling regimes: implications for diatom blooms. *Limnol. Oceanogr.* **46**, 1661–1674. http://dx.doi.org/10.4319/lo.2001.46.7.1661.

Cameron V. and Vance D. (2014) Heavy nickel isotope compositions in rivers and the oceans. *Geochim. Cosmochim. Acta* **128**, 195–211. http://dx.doi.org/10.1016/j.epsl.2005.05.022.

Chapman J. B., Mason T. F. D., Weiss D. J., Coles B. J. and Wilkinson J. J. (2006) Chemical separation and isotopic variations of Cu and Zn from five geological reference materials. *Geostandard. Geoanal. Res.* **30**, 5–16. http://dx.doi.org/10.1111/j.1751-908X.2006.tb00907.x.

Chu N. C., Johnson C. M., Beard B. L., German C. R., Nesbitt R. W., Frank M., Bohn M., Kubik P. W., Usui A. and Graham I. (2006) Evidence for hydrothermal venting in Fe isotope compositions of the deep Pacific Ocean through time. *Earth Planet. Sci. Lett.* **245**, 202–217, 0.1016/j.epsl.2006.02.043.

Coale K. H., Johnson K. S., Fitzwater S. E., Gordon R. M., Tanner S., Chavez F. P., Ferioli L., Sakamoto C., Rogers P., Millero F. J., Steinberg P., Nightingale P., Cooper D., Cochlan W. P., Landry M. R., Constantinou J., Rollwagen G., Trasvina A. and Kudela R. M. (1996) A massive phytoplankton bloom induced by an ecosystem-scale iron fertilization experiment in the equatorial Pacific Ocean. *Nature* **383**, 495–501. http://dx.doi.org/10.1038/383495a0.

Conway T. M. and John S. G. (2014a) Quantification of dissolved iron sources to the North Atlantic Ocean. *Nature* **511**, 212–215. http://dx.doi.org/10.1038/nature13482.

Conway T. M. and John S. G. (2014b) The biogeochemical cycling of zinc and zinc isotopes in the North Atlantic Ocean. *Global Biogeochem. Cycles* **28**, 1111–1128. http://dx.doi.org/10.1002/2014GB004862.

Conway T. M. and John S. G. (2015) Biogeochemical cycling of cadmium isotopes along a high-resolution section through the North Atlantic Ocean. *Geochim. Cosmochim. Acta* **148**, 269–283. http://dx.doi.org/10.1016/j.gca.2014.09.032.

Conway T. M., Rosenberg A. D., Adkins J. F. and John S. G. (2013) A new method for precise determination of iron, zinc and cadmium stable isotope ratios in seawater by double-spike mass spectrometry. *Anal. Chim. Acta* **793**, 44–52. http://dx.doi.org/10.1016/j.aca.2013.07.025.

Coutard A., Meheut M., Vers J., Rols J.-L. and Pokrovsky O. S. (2014) Zn isotope fractionation during interaction with phototrophic biofilm. *Chem. Geol.* **390**, 46–60. http://dx.doi.org/10.1016/j.chemgeo.2014.10.004.

Cutter G. A. and Bruland K. W. (2012) Rapid and noncontaminating sampling system for trace elements in global ocean surveys. *Oceanogr. Limnol. Methods* **10**, 425–436. http://dx.doi.org/10.4319/lom.2012.10.425.

de Souza G. F., Reynolds B. C., Johnson G. C., Bullister J. L. and Bourdon B. (2012a) Silicon stable isotope distribution traces Southern Ocean export of Si to the eastern South Pacific thermocline. *Biogeosciences* **9**, 4199–4213. http://dx.doi.org/10.5194/bg-9-4199-2012.

de Souza G. F., Reynolds B. C., Rickli J., Frank M., Saito M. A., Gerringa L. J. A. and Bourdon B. (2012b) Southern Ocean control of silicon stable isotope distribution in the deep Atlantic Ocean. *Global Biogeochem. Cycle* **26**. http://dx.doi.org/10.1029/2011GB004141.

Dideriksen K., Baker J. A. and Stipp S. L. S. (2008) Equilibrium Fe isotope fractionation between inorganic aqueous Fe (III) and the siderophore complex, Fe (III)-desferrioxamine B. *Earth Planet. Sci. Lett.* **269**, 280–290. http://dx.doi.org/10.1016/S0304-4203(97)00043-1.

Elrod V. A., Berelson W. M., Coale K. H. and Johnson K. S. (2004) The flux of iron from continental shelf sediments: a missing source for global budgets. *Geophys. Res. Lett.* **31**, L12307. http://dx.doi.org/10.1029/2004GL020216.

Ellwood M. J., Hutchins D. A., Lohan M. C., Milne A., Nasemann P., Nodder S. D., Sander S. G., Strzepek R., Wilhelm S. W. and

Boyd (2015) Iron stable isotopes track pelagic iron cycling during a subtropical phytoplankton bloom. *Proc. Natl. Acad. Sci. U.S.A.* **112**(1), E15–E20. http://dx.doi.org/10.1073/pnas.1421576112.

Fitzsimmons J. N., Conway T. M., John S. G. and Boyle E. A. (2013) Iron isotopes in seawater from the Southeast Pacific and North Atlantic Oceans. *Mineral. Mag.* **77**, 1092.

Fitzsimmons J. N., Boyle E. A. and Jenkins W. J. (2014) Distal transport of dissolved hydrothermal iron in the deep South Pacific Ocean. *Proc. Natl. Acad. Sci. U.S.A.* **111**, 16654–16661. http://dx.doi.org/10.1073/pnas.1418778111.

Homoky W. B., Severmann S., Mills R. A., Statham P. J. and Fones G. R. (2009) Pore-fluid Fe isotopes reflect the extent of benthic Fe redox recycling: evidence from continental shelf and deep-sea sediments. *Geology* **37**, 751–754. http://dx.doi.org/10.1130/G25731A.1.

Homoky W. B., John S. G., Conway T. M. and Mills R. A. (2013) Distinct iron isotopic signatures and supply from marine sediment dissolution. *Nat. Commun.* **4**, 2143. http://dx.doi.org/10.1038/ncomms3143.

Horner T. J., Lee R. B. Y., Henderson G. M. and Rickaby R. E. M. (2013) Nonspecific uptake and homeostasis drive the oceanic cadmium cycle. *Proc. Natl. Acad. Sci. U.S.A.* **110**, 2500–2505. http://dx.doi.org/10.1073/pnas.1213857110.

Horner T. J., Williams H. M., Hein J. R., Saito A. M., Burton K. W., Halliday A. N. and Nielsen S. G. (2014) Persistence of deeply sourced iron in the Pacific Ocean. *Proc. Natl. Acad. Sci. U.S.A.* **112**, 1292–1297. http://dx.doi.org/10.1073/pnas.1420188112.

Janssen D. J. and Cullen J. T. (2015) Decoupling of zinc and silicic acid in the subarctic northeast Pacific interior. *Mar. Chem.*. http://dx.doi.org/10.1016/j.marchem.2015.03.014.

Janssen D. J., Conway T. M., John S. G., Christian J., Kramer D. I., Pederson T. F. and Cullen J. T. (2014) An undocumented water column sink for cadmium in open ocean oxygen deficient zones. *Proc. Natl. Acad. Sci. U.S.A.* **111**, 6888–6893. http://dx.doi.org/10.1073/pnas.1402388111.

Jeandel C., Peucker-Ehrenbrink B., Jones M., Pearce C., Oelkers E. H., Godderis Y., Lacan F., Aumont O. and Arsouze T. (2011) Ocean margins: the missing term in oceanic element budgets? *Eos Trans. AGU* **92**, 217. http://dx.doi.org/10.1029/2011EO260001.

Jickells T. D., An Z. S., Andersen K. K., Baker A. R., Bergametti G., Brooks N., Cao J. J., Boyd P. W., Duce R. A., Hunter K. A., Kawahata H., Kubilay N., laRoche J., Liss P. S., Mahowald N. M., Prospero J. M., Ridgwell A. J., Tegen I. and Torres R. (2005) Global iron connections between desert dust, ocean biogeochemistry, and climate. *Science* **308**, 67–71. http://dx.doi.org/10.1126/science.1105959.

John S. G. (2007) Marine biogeochemistry of zinc isotopes. Ph. D. thesis, Woods Hole Oceanographic Institution & Massachusetts Institute of Technology.

John S. G. (2012) Optimizing sample and spike concentrations for isotopic analysis by double-spike ICPMS. *J. Anal. At. Spectrom.* **27**, 2123–2131. http://dx.doi.org/10.1039/C2JA30215B.

John S. G. and Adkins J. F. (2012) The vertical distribution of iron stable isotopes in the North Atlantic near Bermuda. *Global Biogeochem. Cycles* **26**, GB2034. http://dx.doi.org/10.1029/2011GB004043.

John S. G. and Conway T. M. (2014) A role for scavenging in the marine biogeochemical cycling of zinc and zinc isotopes. *Earth Planet. Sci. Lett.* **394**, 159–167. http://dx.doi.org/10.1016/j.epsl.2014.02.053.

John S. G., Geis R. W., Saito M. A. and Boyle E. A. (2007a) Zinc isotope fractionation during high-affinity and low-affinity zinc transport by the marine diatom Thalassiosira oceanica. *Limnol. Oceanogr.* **52**, 2710–2714. http://dx.doi.org/10.4319/lo.2007.52.6.2710.

John S. G., Genevievepark J., Zhang Z., Boyle E. A., Park J. G. and Zhan Z. T. (2007b) The isotopic composition of some common forms of anthropogenic zinc. *Chem. Geol.* **245**, 61–69. http://dx.doi.org/10.1016/j.chemgeo.2007.07.024.

John S. G., Mendez J., Moffett J. W. and Adkins J. F. (2012) The flux of iron and iron isotopes from San Pedro Basin sediments. *Geochim. Cosmochim. Acta* **93**, 14–29. http://dx.doi.org/10.1016/j.gca.2012.06.003.

Johnson K. S., Chavez F. P. and Friederich G. E. (1999) Continental-shelf sediment as a primary source for coastal phytoplankton. *Nature* **398**, 697–700. http://dx.doi.org/10.1038/19511.

Johnson K. S., Gordon R. M. and Coale K. H. (1997) What controls dissolved iron concentrations in the world ocean? *Mar. Chem.* **57**, 137–161. http://dx.doi.org/10.1016/S0304-4203(97)00043-1.

Johnson C. M., Skulan J. L., Beard B. L., Sun H., Nealson K. H. and Braterman P. S. (2002) Isotopic fractionation between Fe(III) and Fe(II) in aqueous solutions. *Earth Planet. Sci. Lett.* **195**, 141–153. http://dx.doi.org/10.1016/S0012-821X(01)00581-7.

Johnson K., Boyle E. A., Bruland K. W., Coale K. H., Measures C. I., Moffett J. W., Aguilar-Islas A. M., Barbeau K., Bergquist B., Bowie A. R., Buck K., Cai Y., Chase Z., Cullen J., Doi T., Elrod V. A., Fitzwater S., Gordon M., King A., Laan P., Baquer L., Landing W. M., Lohan M. C., Mendez J., Milne A., Obata H., Ossiander L., Plant J., Sarthou G., Sedwick P. N., Smith G., Sohst B., Tanner S., Berg van den C. and Wu J. F. (2007) Developing standards for dissolved iron in seawater. *Eos Trans. AGU* **88**, 131–132. http://dx.doi.org/10.1029/2007EO110003.

Kim T., Obata H., Kondo Y., Ogawa H. and Gamo T. (2015) Distribution and speciation of dissolved zinc in the western North Pacific and its adjacent seas. *Mar. Chem.*. http://dx.doi.org/10.1016/j.marchem.2014.10.016.

King A. L. and Barbeau K. A. (2011) Dissolved iron and macronutrient distributions in the southern California Current System. *J. Geophys. Res.* **116**, C03018. http://dx.doi.org/10.1029/2010JC006324.

Koroleff F. (1983) Determination of nutrients. In *Methods of Seawater Analysis* (eds. K. Grasshof, M. Ehrherd and K. Kremling). Verlag Chemie, Weinheim, p. 125.

Labatut M., Lacan F., Pradoux C., Chmeleff J., Radic A., Murray J. W., Poitrasson F., Johansen A. M. and Thil F. (2014) Iron sources and dissolved-particulate interactions in the seawater of the Western Equatorial Pacific, iron isotope perspective. *Global Biogeochem. Cycles* **28**, 1044–1065. http://dx.doi.org/10.1002/2014GB004928.

Lacan F., Francois R., Ji Y. C. and Sherrell R. M. (2006) Cadmium isotopic composition in the ocean. *Geochim. Cosmochim. Acta* **70**, 5104–5118. http://dx.doi.org/10.1002/2014GB004928.

Lacan F., Radic A., Jeandel C., Poitrasson F., Sarthou G., Pradoux C. and Freydier R. (2008) Measurement of the isotopic composition of dissolved iron in the open ocean. *Geophys. Res. Lett.* **35**, L24610. http://dx.doi.org/10.1029/2008GL035841.

Little S. H., Vance D., Walker-Brown C. and Landing W. M. (2014) The oceanic mass balance of copper and zinc isotopes, investigated by analysis of their inputs, and outputs to ferromanganese oxide sediments. *Geochim. Cosmochim. Acta* **125**, 673–693. http://dx.doi.org/10.1029/2008GL035841.

Lupton J. (1998) Hydrothermal helium plumes in the Pacific Ocean. *J. Geophys. Res.* **103**, 15853–15868. http://dx.doi.org/10.1029/98JC00146.

Lynn R. J. and Simpson J. J. (1987) The California current system: the seasonal variability of its physical characteristics. *J. Geophys. Res.* **92**, 12947. http://dx.doi.org/10.1029/JC092iC12p12947.

Maréchal C. N., Nicolas E., Douchet C. and Albarède F. (2000) Abundance of zinc isotopes as a marine biogeochemical tracer. *Geochem. Geophys. Geosyst.* **1**, 1015. http://dx.doi.org/10.1029/1999GC000029.

Moore J. K. and Braucher O. (2008) Sedimentary and mineral dust sources of dissolved iron to the world ocean. *Biogeoscience* **5**, 631–656. http://dx.doi.org/10.5194/bg-5-631-2008.

Moore J. K., Doney S. C. and Lindsay K. (2004) Upper ocean ecosystem dynamics and iron cycling in a global three-dimensional model. *Global Biogeochem. Cycles* **18**, GB4028. http://dx.doi.org/10.1029/2004GB002220.

Moore J. K., Doney S. C., Glover D. M. and Fung I. Y. (2001) Iron cycling and nutrient-limitation patterns in surface waters of the World Ocean. *Deep. Sea Res. Part II* **49**, 463–507. http://dx.doi.org/10.1016/S0967-0645(01)00109-6.

Morel F. M. M. and Price N. M. (2003) The biogeochemical cycles of trace metals in the oceans. *Science* **300**, 944–947. http://dx.doi.org/10.1126/science.1083545.

Morgan J. L., Wasylenki L. E., Nuester J. and Anbar A. D. (2010) Fe isotope fractionation during equilibration of Fe – organic complexes. *Environ. Sci. Technol.* **44**(16), 6095–6101. http://dx.doi.org/10.1021/es100906z.

Nishioka J., Ono T., Saito H., Nakatsuka T., Takeda S., Yoshimura T., Suzuki K., Kuma K., Nakabayashi S., Tsumune D., Mitsudera H., Johnson W. K. and Tsuda A. (2007) Iron supply to the western subarctic Pacific: importance of iron export from the Sea of Okhotsk. *J. Geophys. Res.* **112**, C10012. http://dx.doi.org/10.1029/2006JC004055.

Parekh P., Follows M. J. and Boyle E. A. (2004) Modeling the global ocean iron cycle. *Global Biogeochem. Cycles* **18**, GB1002. http://dx.doi.org/10.1029/2003GB002061.

Radic A., Lacan F. and Murray J. W. (2011) Iron isotopes in the seawater of the equatorial Pacific Ocean: new constraints for the oceanic iron cycle. *Earth Planet. Sci. Lett.* **306**, 1–10. http://dx.doi.org/10.1016/j.epsl.2011.03.015.

Reid, J. L., Roden, G. I. and Wyllie, J. G. (1958) Studies of the California Current system. California Cooperative Oceanic Fisheries Investigations Report 6, pp. 28-56.

Rehkämper M., Wombacher F., Horner T. J. and Xue Z. (2012) Natural and anthropogenic Cd isotope variations. In *Handbook of Environmental Isotope Geochemistry Advances in Isotope Geochemistry.* pp. 125–154. doi:10.1007/978-3-642-10637-8_8.

Ripperger S. and Rehkämper M. (2007) Precise determination of cadmium isotope fractionation in seawater by double spike MC-ICPMS. *Geochim. Cosmochim. Acta* **71**, 631–642. http://dx.doi.org/10.1016/j.epsl.2007.07.034.

Ripperger S., Rehkämper M., Porcelli D. and Halliday A. N. (2007) Cadmium isotope fractionation in seawater – a signature of biological activity. *Earth Planet. Sci. Lett.* **261**, 670–684. http://dx.doi.org/10.1016/j.epsl.2007.07.034.

Saito M. A., Noble A. E., Tagliabue A., Goepfert T. J., Lamborg C. H. and Jenkins W. J. (2013) Slow-spreading submarine ridges in the South Atlantic as a significant oceanic iron source. *Nat. Geosci.* **6**, 775–779. http://dx.doi.org/10.1038/ngeo1893.

Sedwick P. N., Sohst B. M., Ussher S. J. and Bowie A. R. (2015) A zonal picture of the water column distribution of dissolved iron(II) during the U.S. GEOTRACES North Atlantic transect cruise (GEOTRACES GA03). *Deep Sea Res. Pt II.* **116**, 166–175. http://dx.doi.org/10.1016/j.dsr2.2014.11.004.

Severmann S., Johnson C. M., Beard B. L., German C. R., Edmonds H. N., Chiba H. and Green D. R. H. (2004) The effect of plume processes on the Fe isotope composition of hydrothermally derived Fe in the deep ocean as inferred from the Rainbow vent site, Mid-Atlantic Ridge, 36°14′N. *Earth Planet. Sci. Lett.* **225**, 63–76. http://dx.doi.org/10.1016/j.epsl.2004.06.001.

Severmann S., McManus J., Berelson W. M. and Hammond D. E. (2010) The continental shelf benthic iron flux and its isotope composition. *Geochim. Cosmochim. Acta* **74**, 3984–4004. http://dx.doi.org/10.1016/j.gca.2010.04.022.

Skulan J. L., Beard B. L. and Johnson C. M. (2002) Kinetic and equilibrium Fe isotope fractionation between aqueous Fe(III) and hematite. *Geochim. Cosmochim. Acta.* **66**, 2995–3015. http://dx.doi.org/10.1016/S0016-7037(02)00902-X.

Staubwasser M., Schoenberg R., von Blanckenburg F., Krüger S. and Pohl C. (2013) Isotope fractionation between dissolved and suspended particulate Fe in the oxic and anoxic water column of the Batlic Sea. *Biogeoscience* **10**, 233–245. http://dx.doi.org/10.5194/bg-10-233-2013.

Tagliabue A., Aumont O. and Bopp L. (2014) The impact of different external sources of iron on the global carbon cycle. *Geophys. Res. Lett.* **41**, 920–926. http://dx.doi.org/10.1002/2013GL059059.

Tagliabue A., Bopp L. and Aumont O. (2009) Evaluating the importance of atmospheric and sedimentary iron sources to Southern Ocean biogeochemistry. *Geophys. Res. Lett.* **36**, L13601. http://dx.doi.org/10.1029/2009GL038914.

Tagliabue A., Bopp L., Dutay J.-C. C., Bowie A. R., Chever F., Jean-Baptiste P., Bucciarelli E., Lannuzel D., Remenyi T., Sarthou G., Aumont O., Gehlen M. and Jeandel C. (2010) Hydrothermal contribution to the oceanic dissolved iron inventory. *Nat. Geosci.* **3**, 252–256. http://dx.doi.org/10.1038/ngeo818.

Talley L. D. (1993) Distribution and formation of North Pacific intermediate water. *J. Phys. Oceanogr.* **23**, 517–537. http://dx.doi.org/10.1175/15200485(1993) 023<0517:DAFONP>2.0.CO;2.

Talley L. D. (2008) Freshwater transport estimates and the global overturning circulation: shallow, deep and throughflow components. *Prog. Oceanogr.* **78**, 257–303. http://dx.doi.org/10.1016/j.pocean.2008.05.001.

Talley L. D., Pickard G. L., Emery W. J. and Swift J. H. (2011) *Descriptive Physical Oceanography*. Elsevier.

Toner B. M., Fakra S. C., Manganini S. J., Santelli C. M., Marcus M. A., Moffett J. W., Rouxel O. J., German C. R. and Edwards K. J. (2009) Preservation of iron(II) by carbon-rich matrices in a hydrothermal plume. *Nat. Geosci.* **2**, 197–201. http://dx.doi.org/10.1038/ngeo433.

Vance D., Zhao Y., Cullen J. and Lohan M. (2012) Zinc Isotopic Data from the NE Pacific Reveals Shallow Recycling. *Mineral. Mag.* **76**, 2486.

Waeles M., Baker A. R., Jickells T. D. and Hoogewerff J. (2007) Global dust teleconnections: aerosol iron solubility and stable isotope composition. *Environ. Chem.* **4**, 233–237. http://dx.doi.org/10.1071/EN07013.

Wu J., Wells M. L. and Rember R. (2011) Dissolved iron anomaly in the deep tropical–subtropical Pacific: evidence for long-range transport of hydrothermal iron. *Geochim. Cosmochim. Acta* **75**, 460–468. http://dx.doi.org/10.1071/EN07013.

Wyatt N. J., Milne A., Woodward E. M. S., Rees A. P., Browning T. J., Bouman H. A., Worsfeld P. J. and Lohan M. C. (2014) Biogeochemical cycling of dissolved zinc along the GEOTRACES South Atlantic transect GA10 at 40°S. *Global Biogeochem. Cyc.*. http://dx.doi.org/10.1002/2013GB004637.

Xue Z. C., Rehkämper M., Schonbachler M., Statham P. J. and Coles B. J. (2012) A new methodology for precise cadmium isotope analyses of seawater. *Anal. Bioanal. Chem.* **402**, 883–893. http://dx.doi.org/10.1007/s00216-011-5487-0.

Xue Z. C., Rehkämper M., Horner T. J., Abouchami W., Middag R., van de Flierdt T. and de Baar H. J. W. (2013) Cadmium isotope variations in the Southern Ocean. *Earth Planet. Sci. Lett.* **382**, 161–172. http://dx.doi.org/10.1016/j.epsl.2013.09.014.

Yang S.-C., Lee D.-C. and Ho T.-Y. (2012) The isotopic composition of cadmium in the water column of the South China Sea. *Geochim. Cosmochim. Acta* **98**, 66–77. http://dx.doi.org/10.1016/j.gca.2012.09.022.

Yucel M., Gartman A., Chan C. S. and Luther G. W. (2011) Hydrothermal vents as a kinetically stable source of iron-sulphide-bearing nanoparticles to the ocean. *Nat. Geosci.* **4**, 367–371. http://dx.doi.org/10.1038/ngeo1148.

Zhao Y., Vance D., Abouchami W. and de Baar H. J. W. (2014) Biogeochemical cycling of zinc and its isotopes in the Southern Ocean. *Geochim. Cosmochim. Acta* **125**, 653–672. http://dx.doi.org/10.1016/j.gca.2013.07.045.

Associate editor: Claudine Stirling